Queensland University of Technology

Masters Project

Using Monte Carlo simulation to predict dose at extended source to surface distance

Author:
Mr. Christopher Mark Poole

Supervisors:
Dr. Andrew Fielding
Dr. Tanya Kairn
Dr. Phil Back
Mr. Darren Cassidy

Submitted to the School of Physical and Chemical Sciences, Queensland University of Technology, in partial fulfilment of the requirements of the degree of Master of Applied Science (Medical Physics).

August 25, 2008

Statement of Authorship

The work contained in this thesis has not been previously submitted for a degree or diploma at any other tertiary educational institution. To the best of my knowledge and belief, this thesis contains no material previously published or written by another person except where due reference is made.

Signature:

Christopher Mark Poole August 25, 2008

Abstract

Monte Carlo simulation for radiotherapy sources is a computationally intensive operation, especially for large geometries; for this reason it is rarely used for the planning or verification of extended source to surface distance (ESSD) treatments such as total body irradiation (TBI). The Royal Brisbane and Women's Hospital has proposed a modification to its current TBI treatment protocol which will allow for computer based treatment planning from CT data sets instead of manual calculation. The aim of this work is to evaluate the performance of Monte Carlo simulations for estimating the dose delivered to a volume at ESSD by comparing simulated results with experimental data.

A simple rectilinear phantom geometry was defined that facilitated a simple simulation configuration as well as practical experimental data collection. Experimental data was collected using a Solid Water/Plastic Water/PMMA phantom positioned at a number of ESSD's between 190 and 400 cm, and irradiated using a clinical linear accelerator operating at 10 MeV. These same experiments were then modelled using the EGSnrc radiation transport Monte Carlo software with BEAMnrc and DOSXYZnrc user codes. All ESSD measurements were normalised to well defined isocentric reference conditions. Precise Monte Carlo models were generated by examining the performance of a number of variance reduction techniques for ESSD geometries. Energy spectra were calculated using Monte Carlo models to investigate the effect of backscatter on the delivered dose to the volume at ESSD, as well as examine the effect of a PMMA build-up screen on the system.

It was found that Monte Carlo simulation for ESSD geometries is capable of predicting the dose to a volume to within 5% of that indicated by experimental data, when the experiment is performed under conditions that are easily simplified, suitable for simulation. Photon splitting demonstrated the greatest ability to reduce model variance (increase model precision) while keeping computational overhead to a minimum. In normalising all ESSD data to isocentric reference conditions, systematic errors in the Monte Carlo simulations were more easily identified. Monte Carlo generated energy spectra also showed that a PMMA build-up screen introduced 35% more electrons into the system, thus increasing the superficial dose to the volume.

Acknowledgements

I would like to thank my supervisors, Dr. Andrew Fielding and Dr. Tanya Kairn for their ongoing support while keeping me out of trouble over the course of this project.

Special thanks goes out to Dr. Phil Back and Mr. Darren Cassidy of the Royal Brisbane and Women's Hospital who facilitated the experimental portions of this work. They both showed great enthusiasm in assisting with the project, even on weekends.

Usage of a clinical linear accelerator was provided by the Royal Brisbane and Women's Hospital, Brisbane, Australia.

Computational resources and services used in this work were provided by the High Performance Computing (HPC) and Research Support Group, Queensland University of Technology (QUT), Brisbane, Australia.

Supervisors

Dr. Andrew Fielding, QUT
Dr. Tanya Kairn, QUT
Dr. Phil Back, RBWH
Mr. Darren Cassidy, RBWH

Contents

List of Figures

List of Tables

List of Abbreviations

CT	Computed Tomography
EGS	Electron Gamma Shower
ESSD	Extended Source to Surface Distance
MC	Monte Carlo
PMMA	Poly(methyl methacrylate)
QUT	Queensland University of Technology
RBWH	Royal Brisbane and Women's Hospital
SAD	Source to Axis Distance
SSD	Source to Surface Distance
SSPD	Source to Scoring Plane Distance
TBI	Total Body Irradiation
TPS	Treatment Planning System

Chapter 1

Background

Isocentric radiotherapy treatments already benefit from computer aided treatment planning. Complex treatments may be designed to incorporate multiple beam angles, intensities and shapes for targeting a highly localised treatment volume with high precision. While the verification of any radiotherapy treatment plan is carried out with manual calculation, it is the introduction of computer aided treatment planning that has enabled complex treatments.

Monte Carlo simulation is a computationally intensive operation, for this reason it can be seen as prohibitively time consuming. A large geometry tends to require more simulation time due to the need for an increased number of particles, the same is true for simulations requiring very high resolution. Access to a super-computing environment or even a small cluster of computers capable of performing many computations in parallel, can significantly improve the performance of a Monte Carlo simulation, potentially allowing for its use as a treatment planning tool.

1.1 Radiotherapy

Radiotherapy is a technique where ionising radiation is used to reduce the proliferation of cells that make up malignant tumours [1, 2]. Typically a treatment will be either curative or palliative and can be performed along with other treatments such as chemotherapy [3]. With the use of modern radiotherapy techniques and advanced treatment planning systems, dose may be delivered to a treatment volume that is of a complex or irregular shape or occluded by critical tissues. Multiple beams and beam intensities can be applied from different positions and angles to build up a 3-dimensional dose distribution within the treatment volume while sparing critical tissues as much as possible [1, 2]. Specialised treatments such as total body irradiation (TBI) require a uniform dose to be delivered to the entire body of a patient, this is usually achieved by shielding radiation sensitive tissues from the beam with compensators and beam modifiers [4, 1]. With increased treatment complexity, computerised treatment planning systems and simulation techniques become more important in

optimising dose delivery to the patient [5].

Ionising radiation, usually photons or electrons, are used to irradiate the tumour volume, the incident radiation depositing its energy causes direct damage to the DNA within the nucleus of a cell [2, 6]. If sufficient damage occurs, the DNA may not be reparable which in turn results in cell mutation or apoptosis (programmed cell death) [2, 6]. Indirect DNA damage can also results from the creation of free radicals, the most significant of which is produced by the ionisation of H_2O, yielding the free radical OH^- [2].

A typical radiotherapy treatment is usually an ongoing intervention performed in sessions over a number of days or weeks; this is known as fractionation. Fractionation allows for post-irradiation recovery of healthy tissues, while having the added benefit of targeting the cells within the treatment volume at different times throughout the cell-cycle, thus increasing the potential to cause maximum damage to the treatment volume [7]. Understanding that the dose delivered to a volume is accumulative over time, treatment fractionation is an effective technique used to apply a very large dose to a volume while the risk of damaging crucial tissues is minimised [8, 3].

In broad terms a curative radiotherapy treatment is one that is designed to eradicate a cancer from a patient. This contrasts with a palliative treatment, where the primary focus is pain reduction; in effect seeking an improvement in quality of life where cure is unattainable. The distinction between these two treatment methodologies also characterises the allowable side effect threshold. Where the primary focus of the treatment is curative, side effects that include mild pain may be tolerated so long as permanent damage is not caused to tissues surrounding the treatment volume. A palliative treatment on the other hand mandates a much lower side effect threshold; the ultimate goal is quality of life improvement. Any side effects that result in unnecessary pain or patient discomfort are avoided [8, 3].

1.2 Total Body Irradiation

Total body irradiation is a clinical radiotherapy technique designed to deliver a uniform dose to a patients entire body. Primarily the technique is used to suppress the immune system prior to bone marrow transplant or for the treatment of diseases such as leukaemia and non-Hodgkin's lymphoma [4, 8, 7, 3]; in this regard TBI is an adjuvant radiotherapy technique where the goal is curative. A TBI treatment is usually fractionated, where one fraction involves two separate irradiations, one from each side of the patient's body. This is known as a bi-lateral treatment. The dose delivered to a patient over the course of the treatment is enough to be lethal without a bone marrow transplant, because of this high dose late side effects may include: sterility, cataracts, growth retardation or neurological toxicity [1].

1.2.1 Patient Setup

Patient position and setup for a TBI treatment is unconventional when compared to common isocentric techniques. For treatments using a linear accelerator, the patient is positioned at an Extended SSD (ESSD) usually around 4 meters to create a very large field. Depending on the clinic, the patient may be side-on lying down or in an up-seated foetal position as in Figure 1.1. To accommodate a taller patient, the primary collimator of the treatment head may be rotated through 45 degrees allowing for the patient to lie across a diagonal of the field. The treatment couch of the linear accelerator is not used for the treatment, it is common for an auxiliary bed to be brought into the treatment room for the purpose.

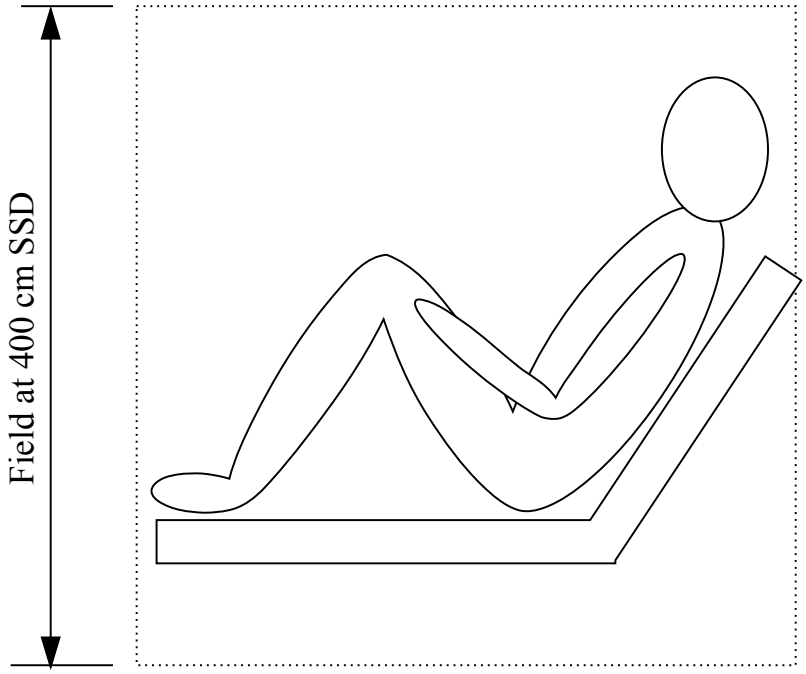

Figure 1.1: Patient positioned in a up-seated foetal position at ESSD

For a TBI, a beam modifier (sometimes referred to as a spoiler) or compensator is a object that is placed in the path of the beam between the source and the patient. These objects perturb the beam such that the delivered dose distribution is changed in some way [4]. The most common beam modifier used in a TBI treatment is a PMMA build-up screen, the screen contaminates the beam with forward scattered electrons so the superficial dose to the patient is increased [4]. The screen is positioned as close to the patient as is possible. Compensators are used to shield radio-sensitive tissues from the beam, such as the head and lungs. A compensator must be carefully designed so the delivered dose to the patient remains as uniform as possible. Generally head and lung compensators will be hung off of the PMMA screen, with their exact position determined by exposing an x-ray film for a short duration; boney landmarks on the patient are then used to improve setup accuracy.

1.2.2 RBWH Current and Future Treatment Protocol

The Royal Brisbane and Women's Hospital (RBWH) currently implements a 400 cm SAD (Source to Axis Distance) bi-lateral treatment with the patient in an up-seated foetal position [9, 10]. Lead compensators are used for shielding of the head and lungs, with the arms of the patient positioned such that lung shielding is further increased. The treatment is delivered with 10 MeV photons at 300 MU/min, a zero-degree primary collimator angle and a 40×40 cm field size [9, 10]. It is a fractionated treatment usually with two fractions being delivered per day for three days. For this current treatment protocol, the prescribed treatment Monitor Units (MU) are calculated manually based on source-to-patient distance with a density correction applied to the lungs, the aim is to achieve a dose uniformity of 10% or less [10].

A proposed modification to the current treatment protocol calls for a rotation of the primary collimator by 45 degrees to accommodate patients being treated in a lying down position with the arms at the side. The motivation for treating patients in such a position is to allow for computerised treatment planning based on CT (Computed Tomography) data sets.

1.3 Monte Carlo Modelling for Radiation Transport

The Monte Carlo Method is a technique used to simulate stochastic systems such as radiation transport [11]. Monte Carlo systems developed specifically for radiation transport are typically highly customisable tools that allow for comprehensive simulations to be performed. A number of MC radiation transport codes are available, some proprietary and others freely distributed or Open Source. It is common for complex simulations to take many hours or days to complete, even in a super-computing environment.

A critical aspect in using Monte Carlo for the modelling of radiotherapy sources is commissioning [12]. Commissioning is effectively the benchmarking process used to ensure a given Monte Carlo model produces results that are comparable to experimental data; it is usually quality assurance (QA) experimental data that is used for commissioning. For a given linear accelerator treatment head, it is manufacturer specification that defines the geometry and material composition of the model [12]. Monte Carlo generated depth doses and dose profiles as well as output factors for a range of field sizes are then calculated and the energy and width of the incident MC electron beam tuned until the simulation agrees with the QA data [13, 14, 15].

Variance reduction is a key element in producing a valid Monte Carlo model [16]. The specifics of the variance reduction techniques vary between MC codes, however the common goal is to produce a more precise model. Generally this is accomplished by introducing more particles into the model while saving computation time by ignoring very low energy

particles that may interact often without depositing significant amounts of energy [17, 18]. To take full advantage of a variance reduction technique, its effect on any particular model must be explored so corruption of reported variance, whether it be over or underestimation, is avoided. Model variance is usually linked to simulation efficiency, where the efficiency of a simulation is a measure of the time taken to produce a model with a particular level of uncertainty [19].

1.3.1 Electron Gamma Shower and User Codes

Electron Gamma Shower or EGSnrc is the de-facto standard for the modelling of clinical radiotherapy sources using Monte Carlo. It is freely available which makes it an attractive research tool. Development started prior to 1991 [20], and since then the code has evolved into a modular radiation transport Monte Carlo platform where custom user codes may be written to exploit its function. Most notably, two user codes, BEAMnrc and DOSXYZnrc, have been developed for the modelling of clinical linear accelerators [21, 22].

BEAMnrc User Code

For the simulation of clinical linear accelerators, BEAMnrc has specific functionality included to create realistic geometric models of a treatment head given a sufficiently detailed manufacturer specification. BEAMnrc produces phasespace files which contain information on particle position, direction, energy and charge, among other parameters, for all particles that cross a scoring plane in the model geometry [21, 23].

DOSXYZnrc User Code

Given a phasespace file produced by BEAMnrc, DOSXYZnrc can model the dose delivered to a user generated phantom or patient CT data set. The user code contains a number of variance reduction tools as well as an interface for building rectilinear voxelised phantoms. The process of voxelising a phantom creates a scoring volume where dose is recorded, groups of voxels are then assigned material properties [22].

Analysis Utilities

EGSnrc, BEAMnrc and DOSXYZnrc provide a number of auxiliary processing utilities to extract useful data from phasespace files and 3D dose files. Readphsp is a phasespace file filtering tool that allows phasespace files to be filtered by particle type. For example, using readphsp, all electrons may be excluded from a phasespace file [22]. BEAMdp is a phasespace file processing tool that generates energy spectra and provides information on other phasespace file characteristics [22].

1.3.2 Extended SSD Simulation

Simulating a complete TBI treatment using Monte Carlo is not routine. Typically dose calculations for such a treatment are performed manually prior to treatment, and adjusted based on measured data collected during each fraction [24]. Previous investigation into the use of Monte Carlo for extended SSD planning is limited to SSD's of between 1.5 and 5 metres [25, 4]. It has been found that inverse square law corrections alone are not sufficient to predict depth doses are extended SSD [25]. Kassaee et al. [4] used MC to examine the dose near the surface during TBI with 15 MeV photons. It was found that the electrons generated in air for short SSD's did not contribute significantly to the entrance dose, whereas electrons introduced into the system at ESSD's up to 5 metres, with the use of a spoiler, were a significant contributor to the entrance dose [4]. Stathakis et al. [25] showed that Monte Carlo simulation can be used to predict the dose to a volume at 1.5 metres SSD to within 1% of predictions made with a Treatment Planning System (TPS).

1.4 Project Objective

The objective of this work is to assess the accuracy and precision of MC based simulation techniques for clinical radiotherapy sources at ESSD. Treatment planning for ESSD treatments such as TBI is usually performed with the aid of manual dose calculations prior to treatment. Using a computer based simulation technique offers an opportunity to greatly improve the efficiency and accuracy of these treatment planning calculations while providing scope for more complex treatments to be implemented. The MC modelling of ESSD radiotherapy techniques presents unique challenges when compared to the modelling of isocentric techniques; especially from a variance reduction and optimisation standpoint.

For simple rectilinear geometries, simulated using the EGS Monte Carlo code for radiation transport, it is hypothesised that Monte Carlo can be used to predict the dose in a volume at ESSD that is in agreement with experimental measurements. Performed in a super-computing environment, it is expected simulations that require very large numbers of particles can be executed significantly faster than if the same simulation where to be performed on a desktop computer.

Chapter 2

Materials and Methods

The precision of a Monte Carlo (MC) model is evaluated by examining the model variance. Similarly the precision of experimental data is evaluated by examining reproducibility. Precise experimental data that has been collected using well practised and well understood methods is considered accurate; a gold standard. A comparison between precise simulated data and a gold standard measures the accuracy of the simulated data. The following details the process of making such a comparison for a Monte Carlo model that simulates a volume at extended source to surface distance (ESSD).

2.1 Experimental Data Collection

Experimentation was carried out using one Elekta Precise clinical linear accelerator on two separate days five weeks apart. On day one the steel framed treatment couch was used as a platform to support the phantom. For day two, a polystyrene (approximately air equivalent) tower was assembled to support the phantom as illustrated in Figure 2.1. All measurements were made with a Farmer ion-chamber (NE 2571) and a Keithley electrometer operating at -250 V.

2.1.1 Reference Measurements

Reference measurements were taken at 100 cm SSD for the 400 cm ESSD measurements, where the steel framed treatment couch was used to support the phantom. The phantom had dimensions of $20 \times 20 \times 21.5$ cm and was made up of solid water and plastic water with a solid water ion-chamber insert. For ESSD measurements at 190 cm and 290 cm, reference measurements were taken at 90 cm SSD. In this instance the phantom was made up of plastic water and solid water as before, but with an ion-chamber insert made of PMMA due to equipment availability limitations. The phantom was supported using the approximately air equivalent polystyrene tower shown in Figure 2.1. The field size for these reference

measurements was 40×40 cm. Both measurements were taken at a depth of 10 cm with 150 MU delivered at 300 MU/minute. Where 1 monitor unit (MU) is equivalent to a dose of 1 cGy delivered in a water phantom on-axis at d_{max} for a 10×10 cm field at 100 cm SSD. Figure 2.2 illustrates the reference phantom position relative to the treatment head, note that the gantry is positioned at zero degrees; a vertical beam delivery.

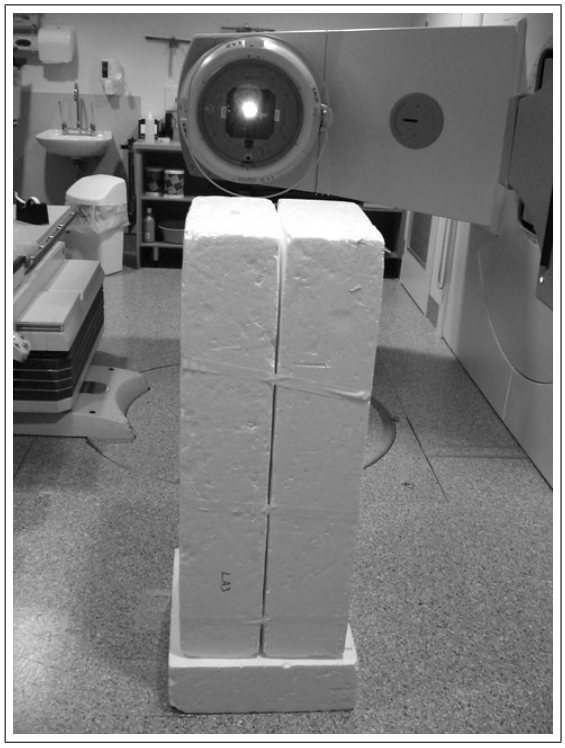

Figure 2.1: Styrene (approximately air equivalent) tower used to position the phantom at ESSD

Figure 2.2: Reference water equivalent phantom setup relative to the treatment head

2.1.2 Depth Doses at Extended SSD

Two depth doses at ESSD without the PMMA screen were recorded, one at 190 cm SSD and another at 290 cm SSD. These measurements used the polystyrene tower to support the phantom, as illustrated in Figure 2.1. The gantry was positioned at 270 degrees for a horizontal beam delivery. All doses were corrected for temperature (23.3 $^{\circ}C$) and pressure (101.44 kPa), and were normalised to the datum measured under reference conditions described in Section 2.1.1. While maintaining a constant SSD, with a number of plastic water sheets of different thickness, it was possible to move the position of the ion-chamber through the phantom by adjusting the order of the sheets. For a number of depths between 10 and 135 mm, the phantom was irradiated with 300 MU at 300 MU/min for a field size of 40×40 cm at both SSD's. Note that for these measurements the ion-chamber phantom insert was made of PMMA.

2.1.3 PMMA Build-up Screen

With the phantom positioned on the patient treatment bed at 400 cm SSD, using a solid water/plastic water composite phantom, the same method used to measure depth doses in Section 2.1.2 was employed to measured depth doses with and without the PMMA build-up screen in position. The screen was positioned as close to the treatment bed as possible, with a distance of 37.3 cm from the surface of the phantom to the rear surface of the screen (see Figure 2.3). For measurements at a depth of 10 cm, the phantom was irradiated with 1000 MU at 300 MU/min for a field size of 40×40 cm; this was performed with and without the PMMA screen in position. In addition to this, 4 measurements were taken with the screen in position, at depths between 8 and 11 mm around d_{max} for 500 MU at 300 MU/min. All doses were corrected for temperature (23.4 $^{\circ}C$) and pressure (100.86 kPa), and were normalised to the datum measured under reference conditions described in Section 2.1.1.

Figure 2.3: Water equivalent phantom at ESSD with PMMA screen in position

2.1.4 Dose Contribution from Backscatter

The dose contribution from backscatter was measured by positioning the ion-chamber, enclosed in a 15 mm PMMA build-up cap at 393 cm SSD, with the primary beam shielded with lead blocks, as illustrated in Figure 2.4. With a field size of 40×40 cm the ion-chamber was irradiated with 300 MU at 300 MU/min.

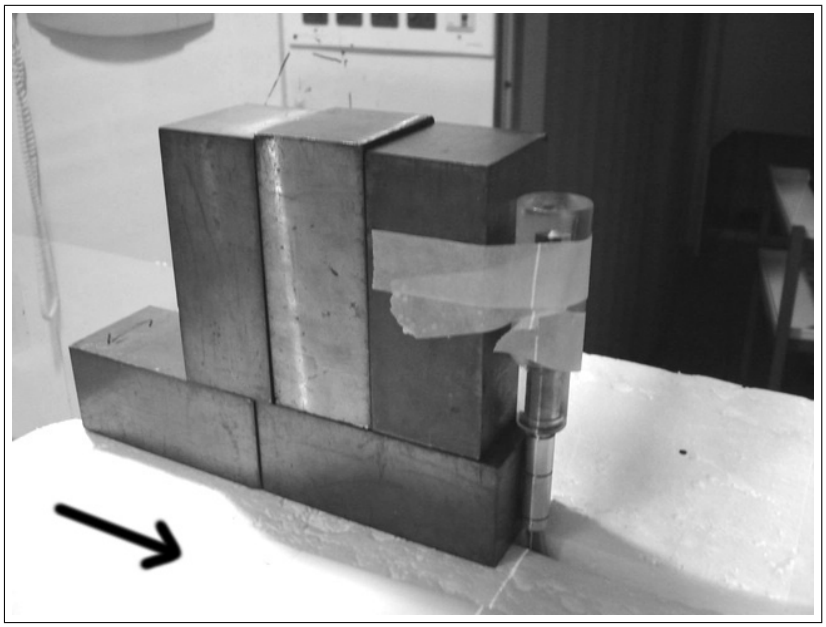

Figure 2.4: Measuring backscatter from the concrete wall behind the treatment area. The arrow indicates the direction of the beam.

2.1.5 Cable Signal

The inclusion of the ion-chamber cable in the path of the beam can cause error in measurement. This is known as cable signal. The ion-chamber, enclosed in a 5 mm Cobalt build-up cap was set up at 297 cm SSD with the primary beam shielded by a number of lead blocks. The ion-chamber was irradiated with 300 MU at 300 MU/min for a field size of 40×40 cm. The process was repeated with approximately double the signal cable included in the beam. The contribution of cable signal was determined from these two measurements.

2.2 Monte Carlo Simulation

Monte Carlo simulation is only a simple reproduction of the experimental conditions, both geometrically and physically. With this in mind it is important to perform experiments that are easy to model and simulate. As a result of software limitations it is not always straightforward to include objects such as the treatment couch or the walls and floor of a treatment room in a simulation. For this study, objects such as the PMMA screen were either excluded from the model or simplified. The following simulations represent the PMMA screen as a plain sheet of PMMA without a frame or structural supports. It should also be noted that the phantom is modelled as water (not water equivalent material) as water is a standard material available in EGSnrc, whereas the Plastic Water and Solid Water equivalents are not.

Although the actual commissioning process is outside of the scope of this study it is important to realise that the model used in this study was commissioned using experimental quality assurance data at or around the isocentre of the linear accelerator. The phasespace file contained on the order of 500 million particles, scored at the exit window of the treatment head. The linear accelerator modelled was an Elekta Precise clinical linear accelerator, based on a 6 MeV model created by Kairn et al. [26] that was modified for 10 MeV output.

Figure 2.5 illustrates the simulation reference geometry, with a $20 \times 20 \times 21.5$ cm water phantom. This geometry is a simplified reproduction of the experimental reference geometry. The treatment couch has been excluded from the simulation reference geometry, as have some other treatment room features, such as the side wall and floor. The reference measurements were taken at a depth of 10 cm for a filed size of 40×40 cm. Two reference simulations were performed, one at 90 cm the other at 100 cm, to model the experimental reference measurements described in Section 2.1.1.

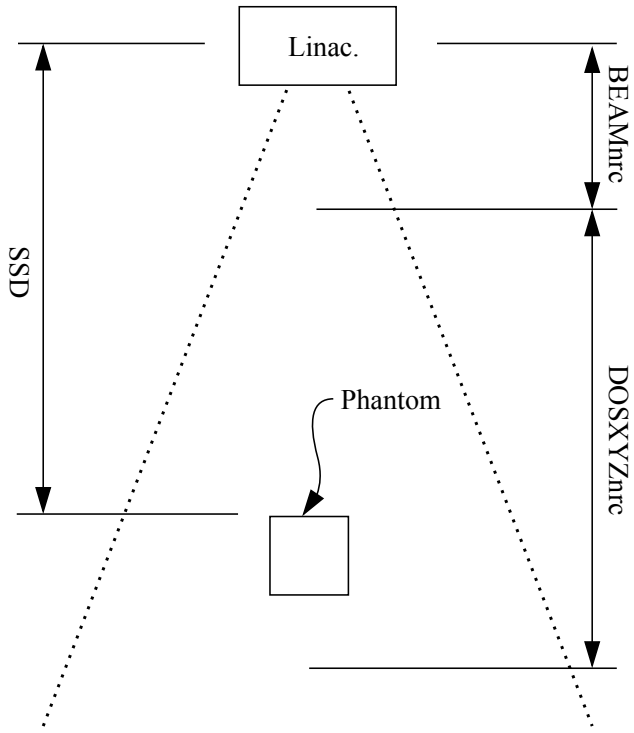

Figure 2.5: Simulation reference geometry schematic

2.2.1 Variance Reduction

Prior to the collection of data from any Monte Carlo simulation for comparison with experimental data, the precision of the simulation technique was evaluated at ESSD. For a generic ESSD model geometry, a range of model simulation and common variance reduction parameters were investigated. The following variance reduction techniques were examined: range rejection, photon splitting, photon recycling and multi-run averaging. All simulations used a phasespace file from a commissioned linear accelerator model with a field size of 40×40 cm, with the phasespace file rotated by 45 degrees to simulate a rotating of the primary collimator by the same angle. The phantom geometry and voxel composition is schematically illustrated in Figure 2.6. The variance of each simulation was taken by calculating the mean and standard deviation of each high resolution on-axis voxel group in the model.

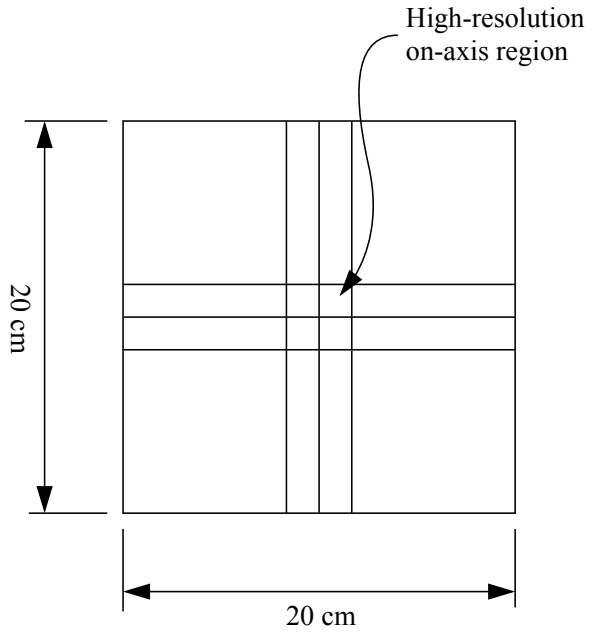

Figure 2.6: Simulated phantom geometry and voxel position optimised for depth dose measurement

Rogers and Mohan [27] define model variance as:

$$s^2 = \frac{1}{n} \sum_{D_i \geq D_{max}/2} \left(\frac{\Delta D_i}{D_i} \right)^2 \tag{2.1}$$

where s^2 is the model variance, n is the number of voxels that have a dose greater than 50% of d_{max}, ΔD is the variance of the current voxel and D is the dose of the current voxel. This is the generally accepted method of determining model variance, however it only holds true for phantoms that have uniform voxels. An optimum design of a phantom used to create depth doses for example, contains a narrow column of small voxels (high resolution) on-axis, with large padding voxels around this column to maintain correct scatter conditions. Large voxels tend to have a lower variance compared to smaller voxel, since larger voxels have relatively greater numbers of particles depositing energy in them. For a phantom that contains a number of voxel sizes, it is more appropriate to only consider the voxels that are used to produce the data of interest.

$$s^2 = \frac{1}{n} \sum_{D_{scored}} \left(\frac{\Delta D_i}{D_i} \right)^2 \tag{2.2}$$

In doing this, it is less likely the calculated model variance will be skewed by considering very large voxels that may be included in a model strictly for producing correct scatter conditions.

Range Rejection

Range rejection is a technique that forces relatively low energy particles to deposit whatever energy they currently possess at at their current location. In practice this is implemented by assessing whether or not the current particle has enough energy to reach and subsequently cross the next voxel boundary. In applying this technique simulation time is reduced; less time is wasted following low energy particles that may not contribute significantly to the recorded dose. The effect of range rejection on model variance was evaluated by varying the cut-off energy (ESAVE in BEAMnrc) over the interval 0.0 to 0.7 MeV and subsequently comparing the resulting model variance for each value of ESAVE.

Photon Splitting

For a splitting number (n_split in BEAMnrc) greater than 1, all primary photons are split into weighted sub-photons n_split times. The weight of any one sub-photon is 1/n_split. Any secondary or scattered particle produced by a sub-photon receives a weight of the original photon, but survives with a probability of 1/n_split. Photon splitting allows for the introduction of more photons into the simulation without the need for a very large phasespace file. The value of n_split was varied between 1 and 100 and with the model variance recorded for each new value of n_split.

Photon Recycling

Particle or photon recycling is a technique where any one individual particle in a phasespace file is introduced into a system NRCYCL times. Recycling differs from photon splitting in that all initial histories are weighted and survive normally; a recycled particle is used as though it is the first time it has been used in the simulation. The recycling number NRCYCL may be implicitly defined and automatically calculated at runtime by specifying a value of i_hist that is greater than the available number of particles in a phasespace file (i_particle). Alternatively the maximum permissible number of times a particle may be recycled can be explicitly defined by setting NRCYCL manually. The affect of photon recycling on model variance was evaluated by varying i_hist between 400×10^6 and 1×10^9.

Multi-run Averaging

Multi-run Averaging is effectively a signal averaging technique where a simulation is performed multiple times with the same parameters and the results combined. The performance of this technique was evaluated by running a simulation 15 times and averaging the results 2 to 15 times. The integers used to seed the random number generator were held constant for one test and adjusted randomly for each run in a second test. In addition to this, the order of averaging and its effect on the results were examined. This was achieved by firstly averaging

the results according to simulation order, and then averaging the results in a random order. The multi-run averaging simulations were performed with a photon splitting number of 70 based on the results described in Section 3.2.

2.2.2 Depth Doses

Depth doses were measured on-axis experimentally, this called for a simulation of a phantom with a high on-axis resolution; similar to the phantom illustrated in Figure 2.6. Included in this simulation geometry was the water phantom, the PMMA build-up screen and the rear wall of the treatment room.

Once the voxels of the phantom have been defined, the relative position of objects can be adjusted by altering the dimensions of the voxels that surround them. Removing an object from the simulation is as simple as setting its material to that of the surrounds; in this case air. Setting an object's material to that of the surrounds preserves the voxel composition of the phantom. This allows for more meaningful comparisons between models that include and exclude certain geometric features. Using these principles, the following simulations were performed.

Depth Doses at ESSD

With the wall and screen modelled as per Figure 2.7, two models were created. The first with the water block at 190 cm SSD (position A in Figure 2.7) and the second with the water block at 290 cm SSD (position B in Figure 2.7). Note that both the concrete wall and PMMA screen were downstream of the water block in each case. Depth doses were calculated by averaging the high resolution on-axis voxel groups at each depth for each model. All data was normalised to the reference simulations described in Section 2.2.

Build-up Screen

To examine the effect of the build-up screen on dose deposited in the water phantom, two simulations were performed, one with the screen in position, and the other with the screen removed. The water phantom was position at 400 cm SSD, shown at position C in Figure 2.7. A depth dose was created from this model in the same manner as previously described. All data was normalised to the reference simulations described in Section 2.2.

Reproducing Scatter Conditions

With the same models used to examine the build-up screen, a concrete wall was included to the rear of the water block as shown in Figure 2.7. Depth doses were then produced to compare the dose delivered to the water block with and without the wall. All data was normalised to the reference simulations described in Section 2.2.

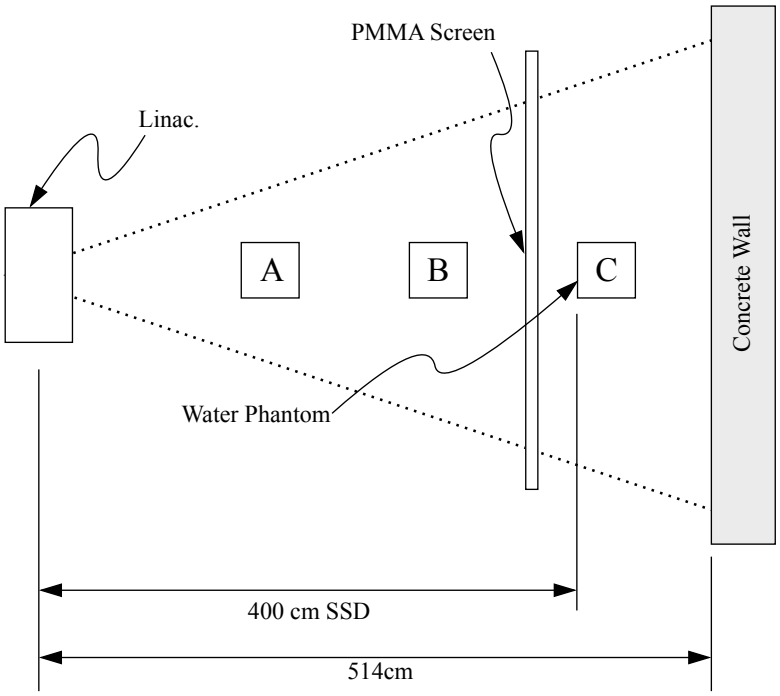

Figure 2.7: Simulated phantom geometry with the concrete wall included in the model. Three phantom positions are shown; 190 cm SSD for A, 290 cm SSD for B and 400 cm SSD for C.

2.2.3 Energy Spectra

Energy spectra are generated from phasespace files positioned at points of interest and processed with BEAMdp. Three extended source to scoring plane distances (SSPD) were used; they were 200, 300 and 400 cm. Figure 2.8 shows the position of these scoring planes relative to the surrounding model geometry. For each SSPD, phasespace files were produced for four different models: with both the PMMA screen and concrete wall, neither the PMMA screen or concrete wall, the PMMA screen only, and the concrete wall only. These 12 phasespace files were processed to generate energy spectra.

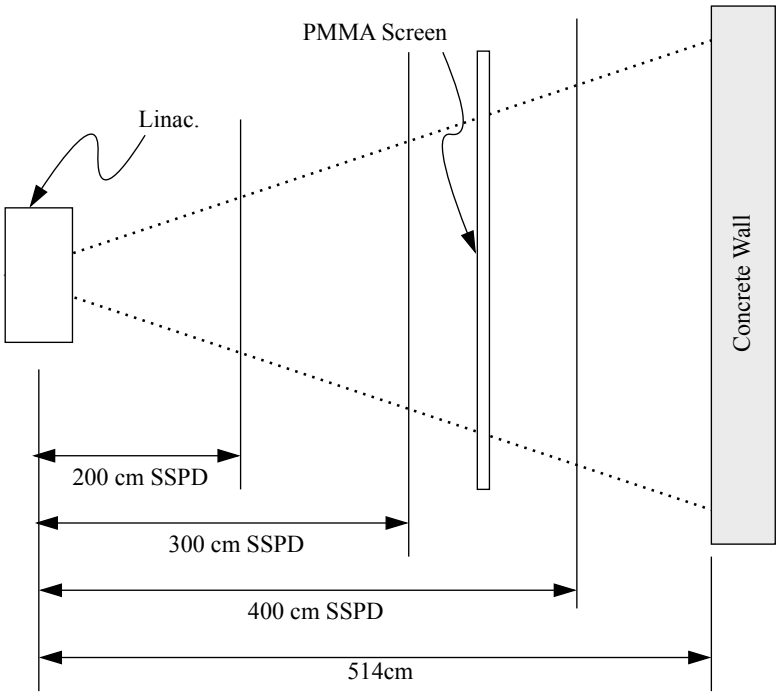

Figure 2.8: Energy spectra scoring planes relative to key model geometries

Full Energy Spectra

For each of the 12 calculated phasespace files, full energy spectra that included all particles, including both back and forward scattered particles, were produced using BEAMdp. The energy window was set to 0.0 to 10.0 MeV using 200 bins.

Low Energy Spectra

So the low energy features of the spectra could be examined, BEAMdp was used to create full energy spectra, this time using an energy window of 0.0 to 1.0 MeV using 200 bins. This was performed for all 12 phasespace files.

Backscatter

In order to properly examine backscatter energy spectra it is necessary to filter out forward-scattered particles from the phasespace file. Included with EGSnrc is readphsp, a tool that allows phasespace files to be filtered. For example, for a given multi-particle phasespace file, a new phasespace file may be produced containing only electrons. The official and most current implementation of readphsp accomplishes this particle filtering by parsing all particles in the input phasespace file through a series of IF statements each testing for a different particle type. For a given particle type test, if the current particle type is TRUE, the current particle is appended to the output phasespace file.

For each SSPD and combination of including and excluding the concrete wall and PMMA screen, backscattered particles were filtered out using readphsp modified for backscatter filtering (readphsp_bs). Energy spectra were then generated using BEAMdp between energies of 0.0 and 0.5 MeV using 200 bins.

For a given particle in a phasespace file, it is considered to be backscattered if it is travelling upstream towards the source; this direction is nominated as the negative z-direction. The sign of the z-direction cosine must be tested for each particle parsed before the particle type is determined as any particle type can be backscattered; this is more computationally efficient. A phasespace file produced by BEAMnrc dose not explicitly contain the z-direction cosine of each particle, it is calculated from the x-direction and y-direction cosines. The sign of the z-direction cosine is attached to the weight of each particle; when particle weight is used for a computation sign is ignored as a negative particle weight has no meaning. To filter out backscatter particles from a phasespace file, only particles with a negative z-direction cosine (negative particle weight) are allowed to be processed for particle type. This method allows for backscattered photons to be filtered out of a multi-particle phasespace file for example.

Electron Contamination

For the models that included both the PMMA screen as well as the concrete wall, all particles except for forward scattered electrons were filtered out of the phasespace files at each SSPD (200, 300 and 400 cm) using readphsp_bs described previously. BEAMdp was then used to generate the energy spectra for an energy window of 0.0 to 10.0 MeV using 200 bins. The affect of the PMMA screen and concrete wall at 400 cm SSPD was then examined by filtering out all particles except for forward scattered electrons from all phasespace files produced at 400 cm SSPD.

Chapter 3

Results

The following presents the results of assessing the Monte Carlo (MC) modelling technique for both accuracy and precision at extended source to surface distance (ESSD) for a limited test case that attempts to simulate a total body irradiation (TBI) treatment. All phasespace files were created using a commissioned BEAMnrc MC model, and all MC dose information was generated with DOSXYZnrc. Experimental data collection was performed at the Royal Brisbane and Women's Hospital.

3.1 Experimental Data Collection

Depth Doses at Extended SSD

Figure 3.1 shows the results of measurements taken at 190 cm, 290 cm and 400 cm SSD. Note that the 190 cm and 290 cm SSD measurements were taken without the PMMA screen and with the phantom supported by the polystyrene tower shown in Figure 2.1, the 400 cm SSD measurements were taken with the PMMA screen in position with the phantom supported by a steel framed treatment bed. All measurements have been corrected for temperature and pressure and normalised to reference conditions as described in Section 2.1.1.

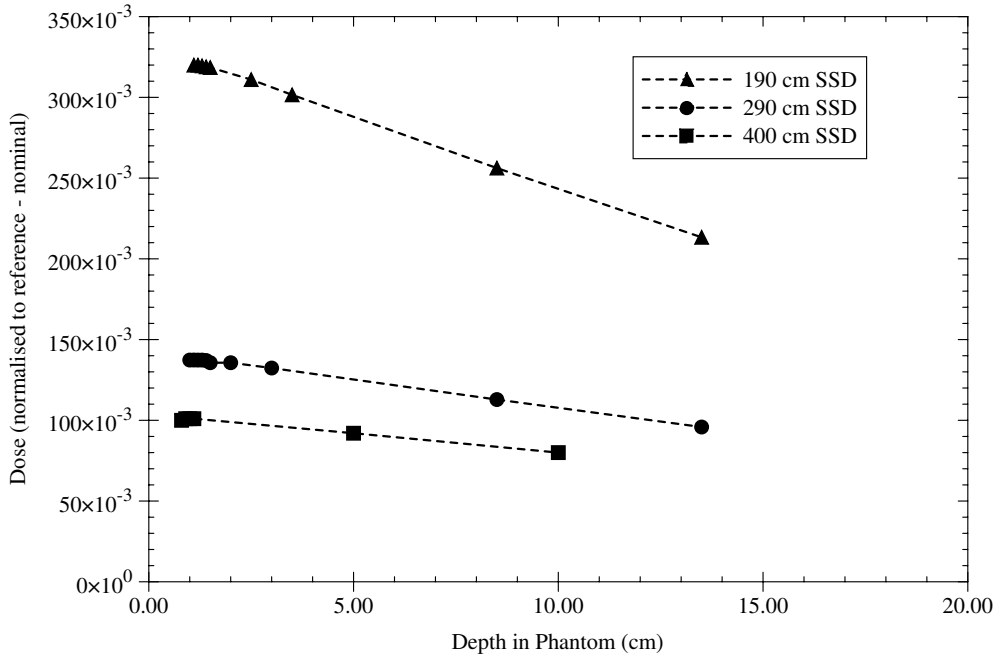

Figure 3.1: Experimental data recorded at 190 cm, 290 cm and 400 cm SSD. Dotted lines interpolated between data as a guide only.

Dose Contribution from Backscatter

Using the method described in Section 2.1.4, the dose contribution from backscatter was measured to be 0.28 nC/nominal nC at 393 cm SSD when irradiated with 300 MU at 300 MU/min. This represents approximately 1.5% of the dose to the Solid Water phantom at 400 cm SSD and a depth of 10 cm.

Cable Signal

Using the method described in Section 2.1.5, the cable signal was measured to be 0.12 nc/nominal nC at 397 cm SSD when irradiated with 300 MU at 300 MU/min. This represents approximately 0.7% of the dose to the Solid Water phantom at 400 cm SSD and a depth of 10 cm.

3.2 Monte Carlo Variance Reduction

Range Rejection

Figure 3.2 shows how model variance changes with varying ESAVE; it is shown along with a measure of total simulation time. Model variance appears to increase with increasing ESAVE, while simulation or computation time remains constant.

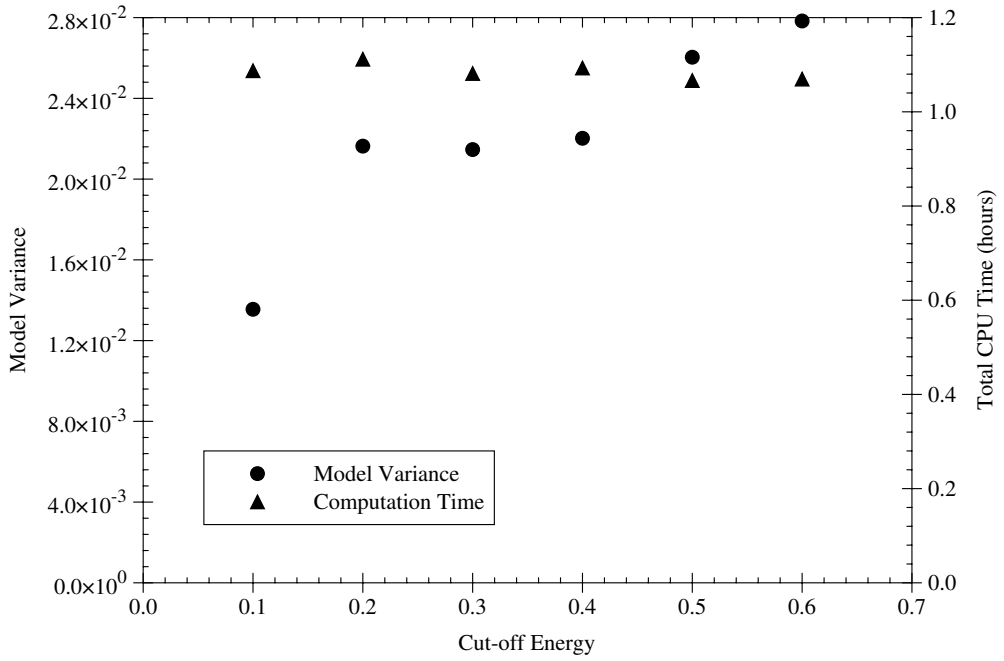

Figure 3.2: Range rejection cut-off energy versus model variance and simulation time.

Photon Splitting Number

Figure 3.3 shows a very rapid reduction in model variance with increasing photon splitting number, flattening off at an n_split of 40 to 60 and greater. Computation time increased linearly with increasing n_split.

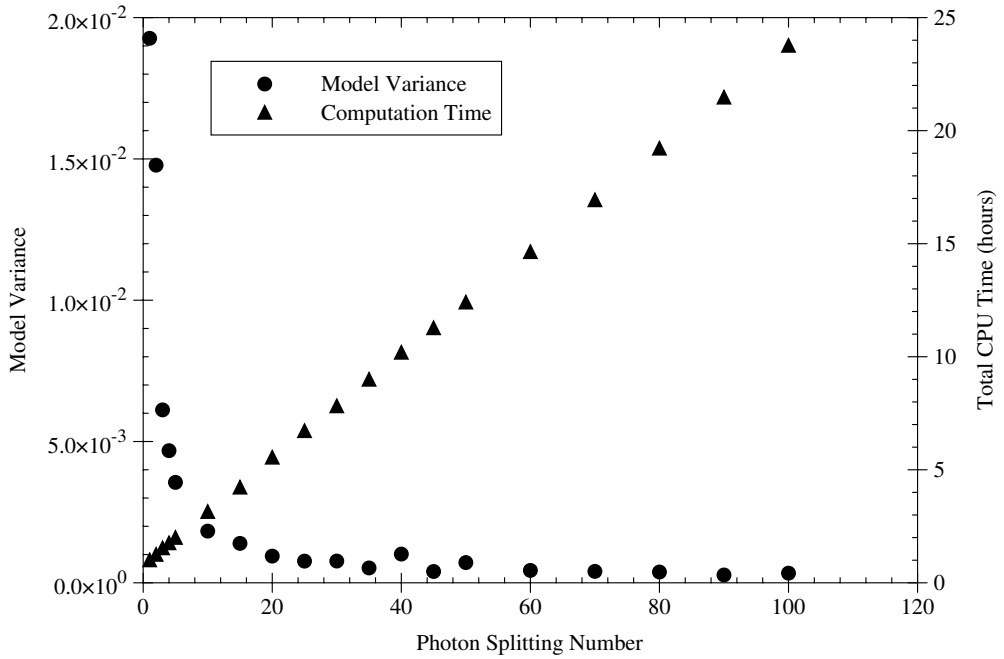

Figure 3.3: Photon splitting number versus model variance and computation time.

Photon Recycling

The photon recycling number (NRCYCL) was configured to be automatically calculated in software at simulation time. For a range of simulated histories (i_hist) greater than the fixed number of available particles in the phasespace file, Figure 3.4 shows model variance for increasing values of i_hist.

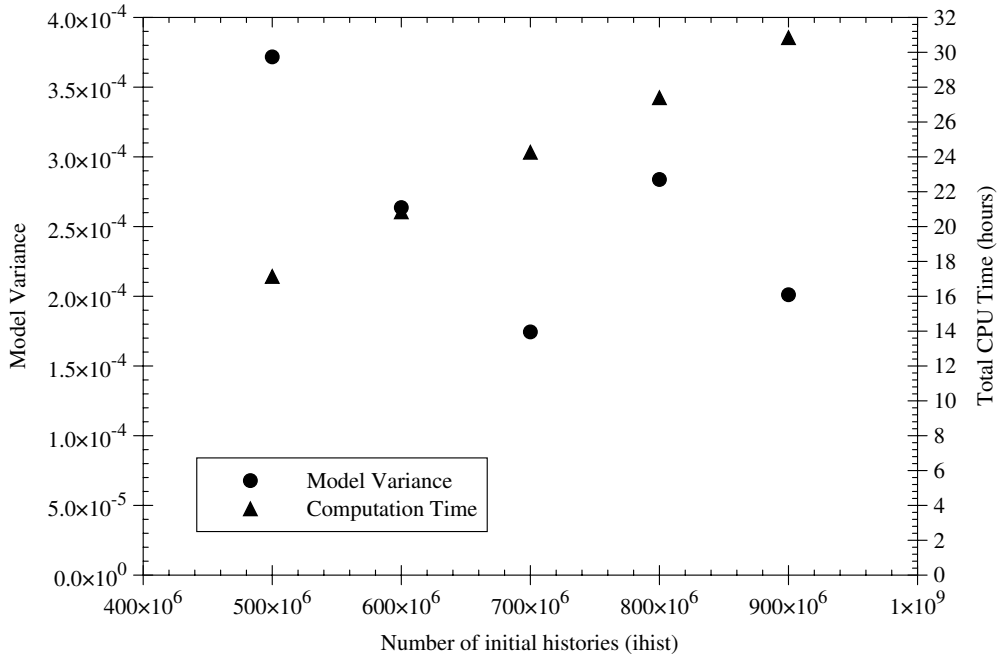

Figure 3.4: The number of initial histories (i_hist) versus model variance and computation time

Multi-run Averaging

The output of multiple runs of the same model may be averaged post simulation. Figure 3.5 shows the results of this technique where the initial random seeds for the simulation were held constant for each run. The performance of this technique was somewhat dependant of the order in which a group of models were averaged. Figure 3.6 uses the same group of models used to generate Figure 3.5 with the order of averaging randomised. Figure 3.7 and 3.8 shows the same technique applied to models where the random seeds were different for each run.

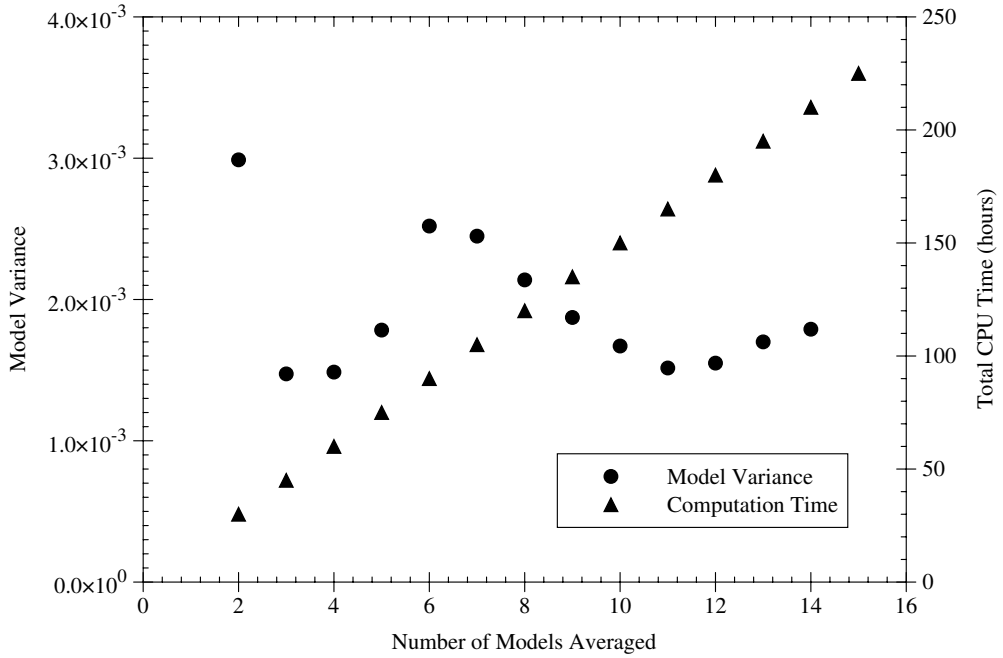

Figure 3.5: Holding random seeds constant; an average of 15 runs of the same model

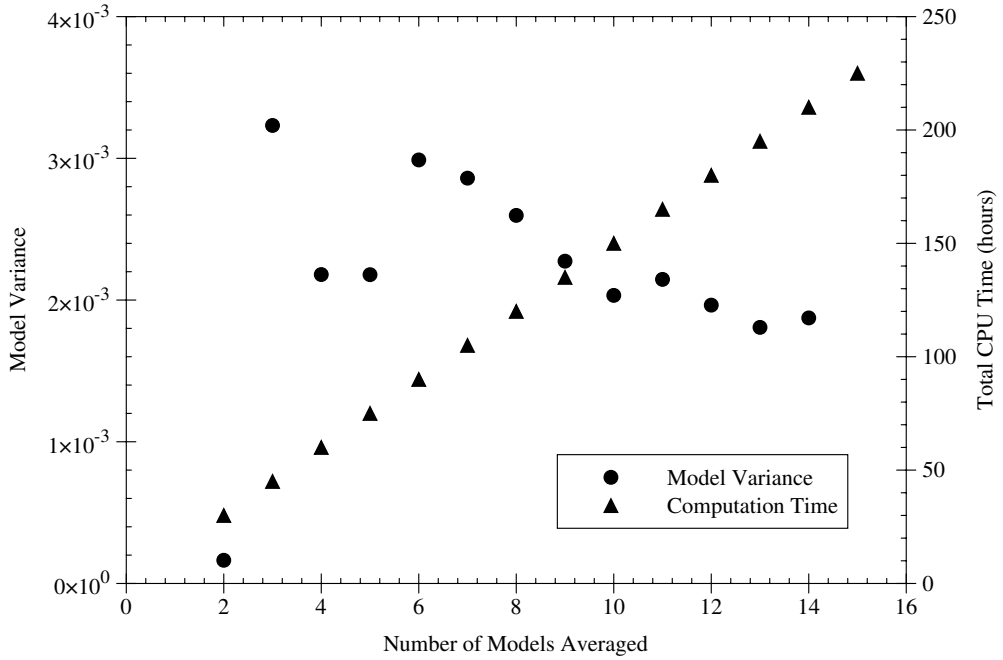

Figure 3.6: Holding random seeds constant; an average of 15 runs of the same model with the order of averaging randomised

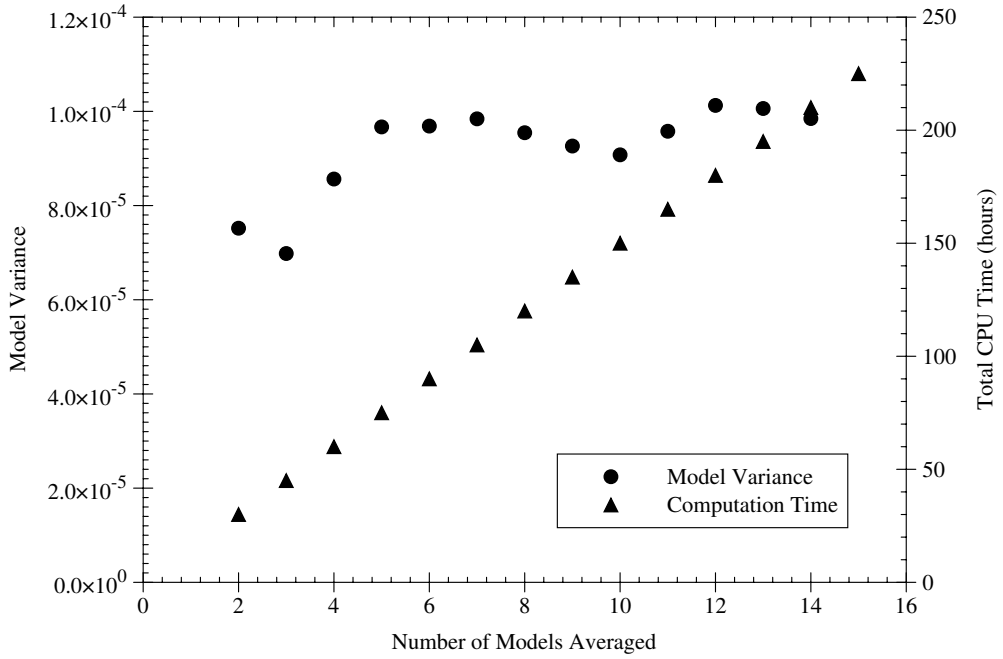

Figure 3.7: Different random seeds for each run; an average of 15 runs of the same model

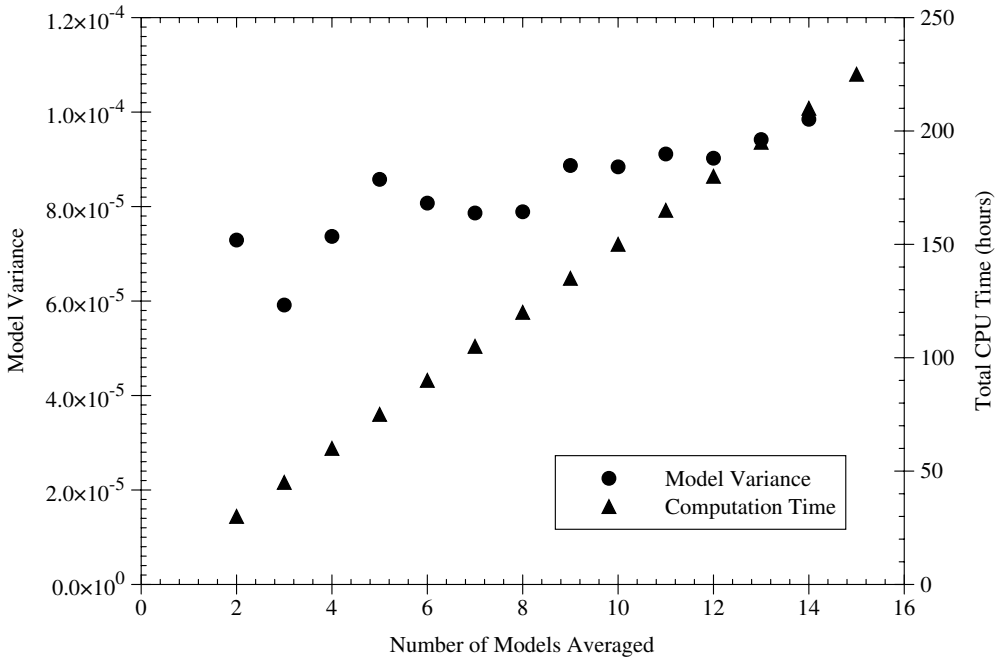

Figure 3.8: Different random seeds for each run; with the order of averaging randomised

3.3 Model Accuracy

A well commissioned model should be both accurate and precise under the reference conditions. The accuracy of the model at ESSD can be evaluated by comparing an ESSD model to equivalent experimental data. The precision of the model at ESSD is improved by employing variance reduction techniques.

Build-up Screen

A typical TBI treatment requires a PMMA screen positioned directly in front of the patient; this screen was also included in the Monte Carlo model. Figure 3.9 shows two Monte Carlo generated depth doses at ESSD with and without the PMMA screen in position. There is a higher phantom entrance dose for the model with the screen included. This is a result of increased forward scattered electron contamination. The screen is positioned 375 cm from the source, with the $20 \times 20 \times 21.5$ cm water phantom positioned at 400 cm SSD. The overlaid experimental data in Figure 3.9 was taken with the PMMA screen in position and with the phantom supported by the steel framed treatment couch; the models are within 10% of this experimental data.

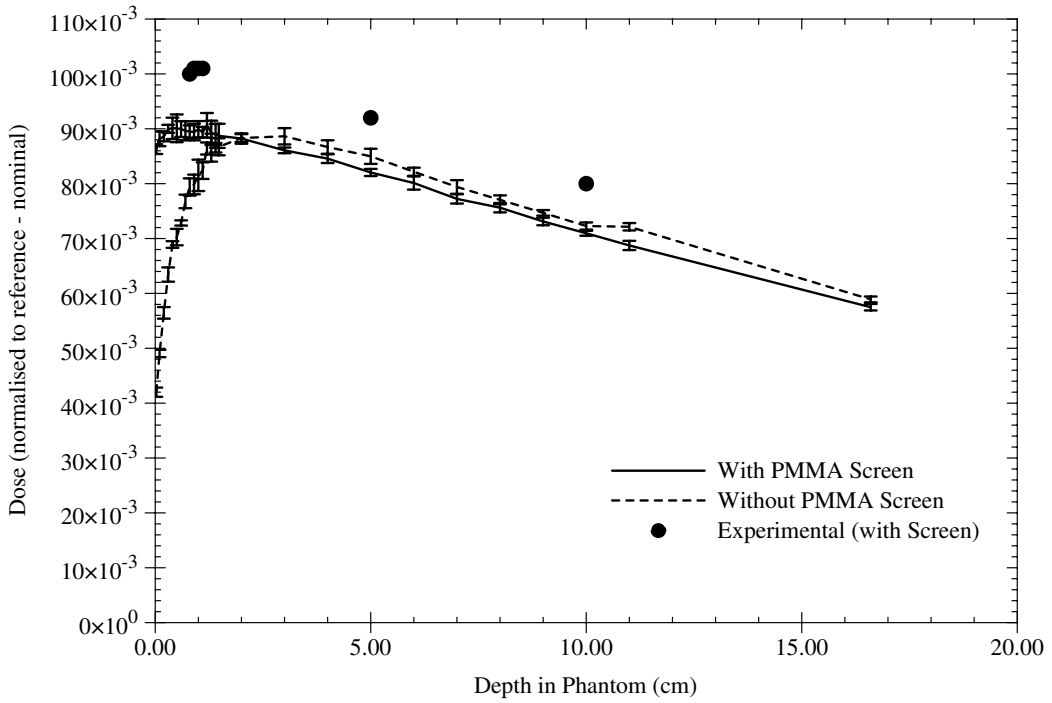

Figure 3.9: Depth dose comparing two Monte Carlo models; one with the PMMA screen in position (model variance of 0.001), the other without the PMMA screen in position (model variance of 0.001). Experimental data is also shown for comparison.

Reproducing Correct Scatter Conditions

In the clinical TBI treatment setting at RBWH, a solid concrete wall is within close proximity behind the patient. The effect this wall has on the dose to a volume at 400 cm SSD is presented in Figure 3.10. When the PMMA screen is included in the model, the effect of the concrete wall appears to be diminished as shown in Figure 3.11. The overlaid experimental data in the following figures was taken with the PMMA screen in position and with the phantom supported by the steel framed treatment couch; the models are within 10% of this experimental data.

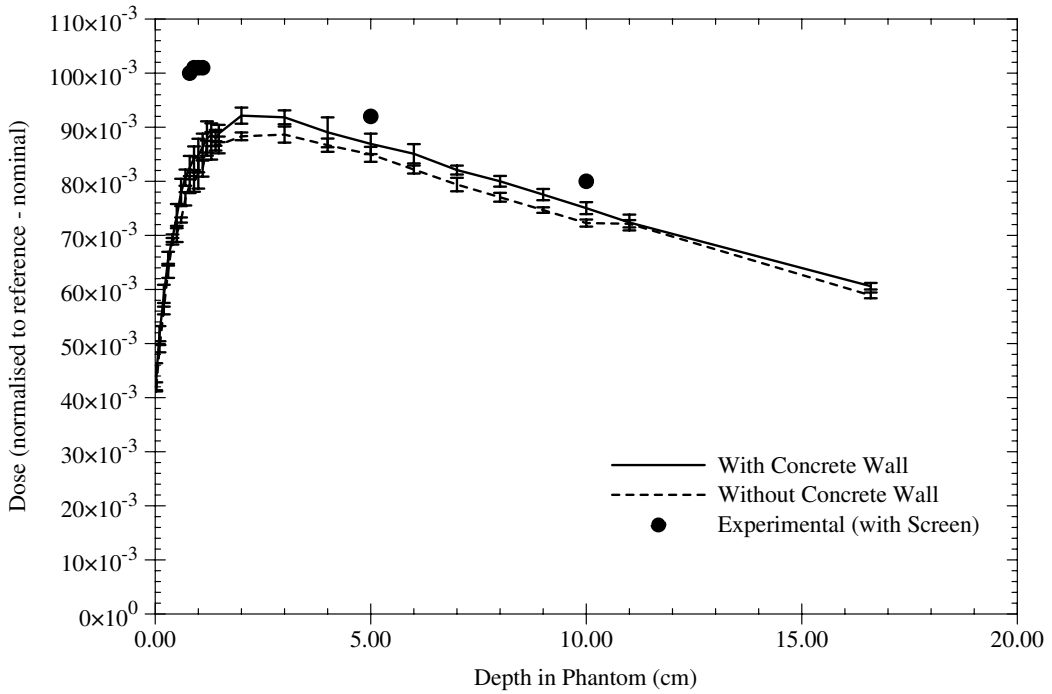

Figure 3.10: Depth Dose in a volume at 400 cm SSD with (model variance of 0.002) and without (model variance of 0.001) the concrete wall in position. Note that the difference between the two sets of simulation results is within the statistical error.

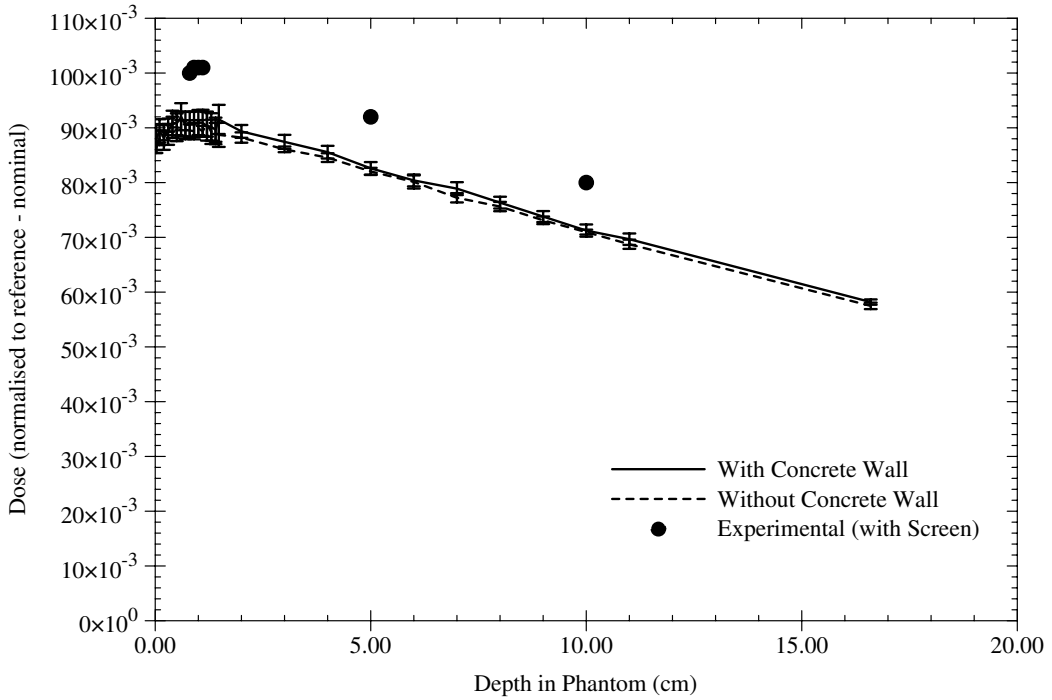

Figure 3.11: Depth Dose in a volume at 400 cm SSD with (model variance of 0.001) and without (model variance of 0.002) the concrete wall in position (with the PMMA screen). The difference between these two sets of simulation results is within the statistical of error.

Depth Doses at ESSD

For ESSD's of 190 cm and 290 cm, experimental depth dose data was collected as described in Section 2.1. These experimental conditions were reproduced with two Monte Carlo models one at 190 cm SSD the other at 290 cm SSD. In Figure 3.12 experimental data has been overlaid for comparison with the MC simulations. All data is normalised to the reference conditions.

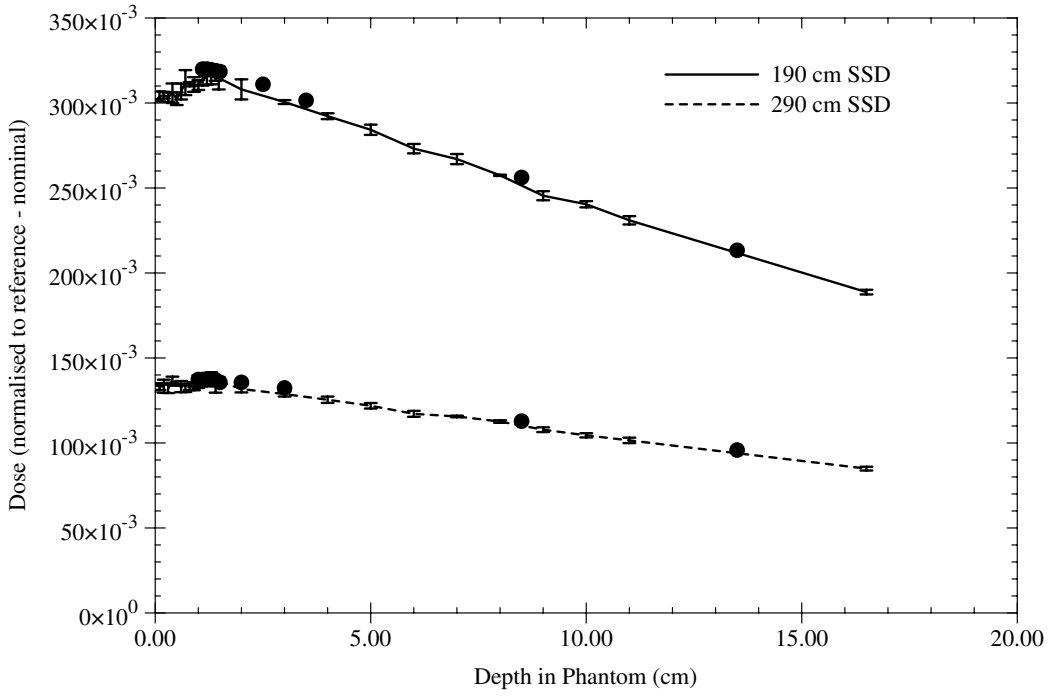

Figure 3.12: ESSD depth doses (190 and 290 cm) with experimental data overlaid; the experimental data was recorded with the screen in position with the phantom supported by the polystyrene tower. The 190 cm SSD model has a model variance of 0.003, and the 290 cm SSD model has a model variance of 0.002. At each SSD, the models are within 5% of the experimental data.

3.4 Energy Spectra at Extended SSD

Using BEAMnrc to simulate the entire system including the treatment head to the concrete wall it is possible to examine the energy spectra of the beam at any point as shown in Figure 2.8. In doing so the effect of beam modifiers and sources of scatter can be examined in terms of energy.

Full Energy Spectra

Figure 3.13, Figure 3.13 and Figure 3.15 show the full energy spectra at 200 cm, 300 cm and 400 cm respectively.

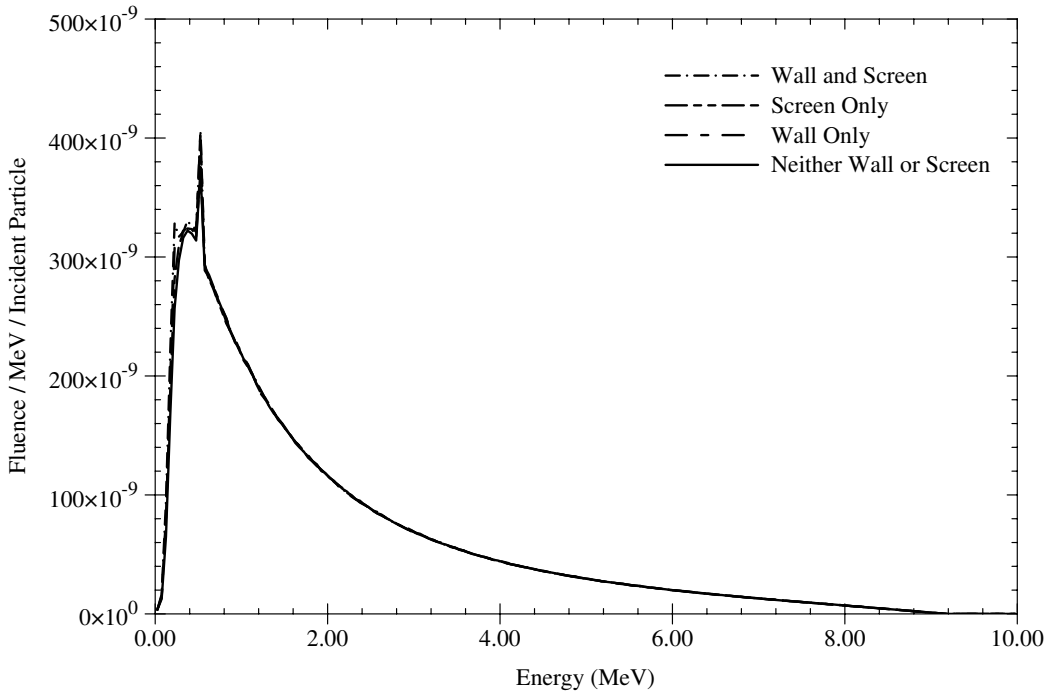

Figure 3.13: All-particle full energy spectra at 200 cm SSPD

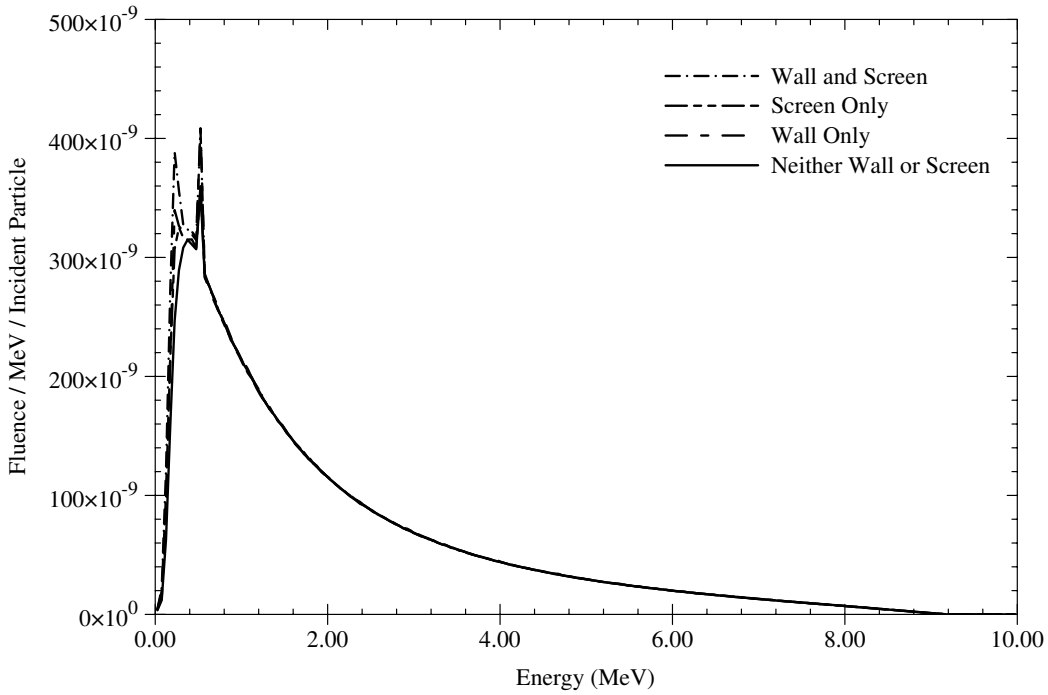

Figure 3.14: All-particle full energy spectra at 300 cm SSPD

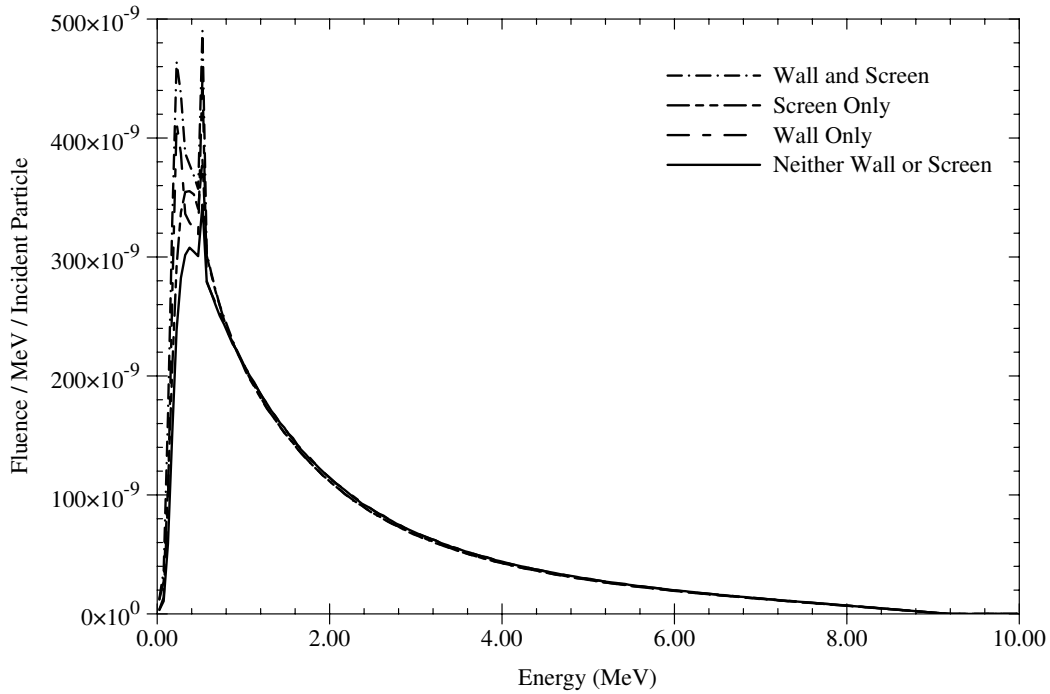

Figure 3.15: All-particle full energy spectra at 400 cm SSPD

In all three of the spectra, there are two defined peaks. One peak is at 511 keV corresponding to the rest mass of an electron, and the other peak is at approximately 220 keV. The 511 keV peak represents the electron-positron annihilation energy and is a standard feature of energy spectra produced from phasespace files using BEAMdp, it has been observed in spectra generated by Markwell [28] and Fix et. al. [29]. The peak around 220 keV is the backscatter peak which is a feature of the model TBI geometry. Figures 3.16, 3.17 and 3.18 below examine this low energy region in more detail.

Low Energy Spectra

Examining the low energy spectra at each of the scoring planes reveal a well defined backscatter peak when the concrete wall is included in the model. The magnitude of this peak increases with decreasing distance between the scoring plane and the concrete wall (increasing SSPD). Note the presence of a peak at 511 keV, this corresponds to the rest mass of an electron; it is produced when an electron annihilates with a positron.

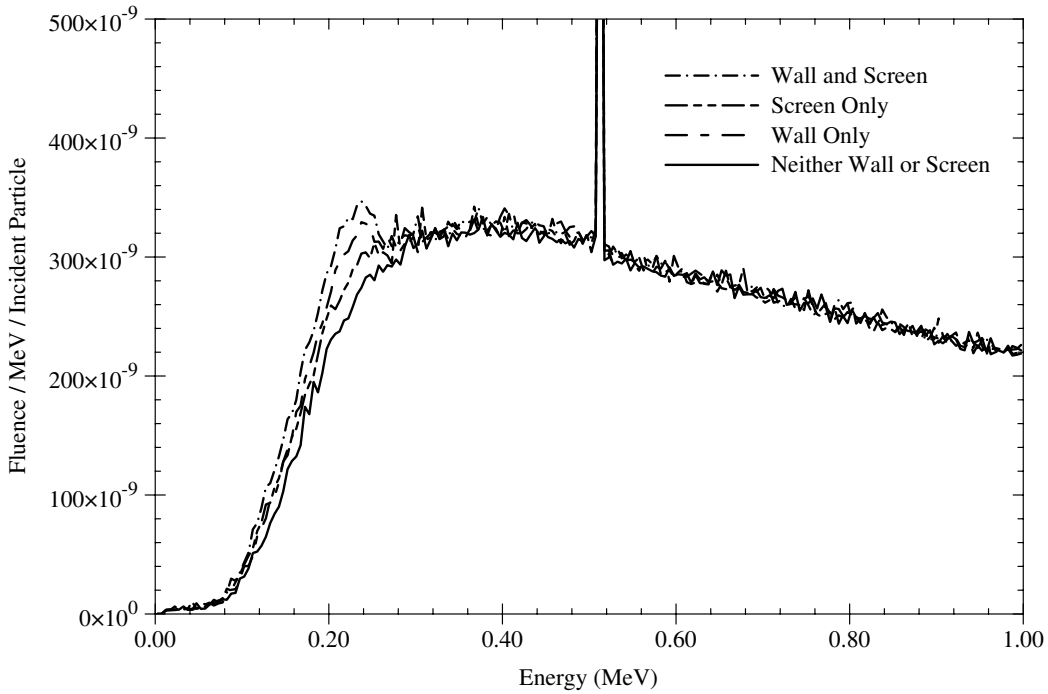

Figure 3.16: All-particle energy spectra (0.0 - 1.0 MeV) at 200 cm SSPD

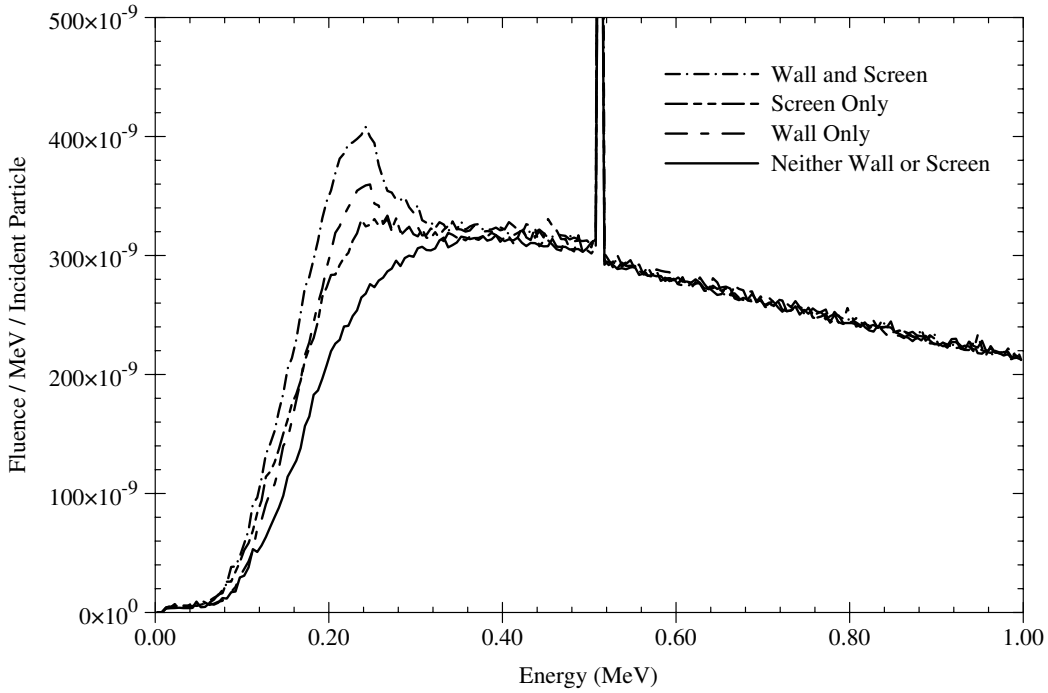

Figure 3.17: All-particle energy spectra (0.0 - 1.0 MeV) at 300 cm SSPD

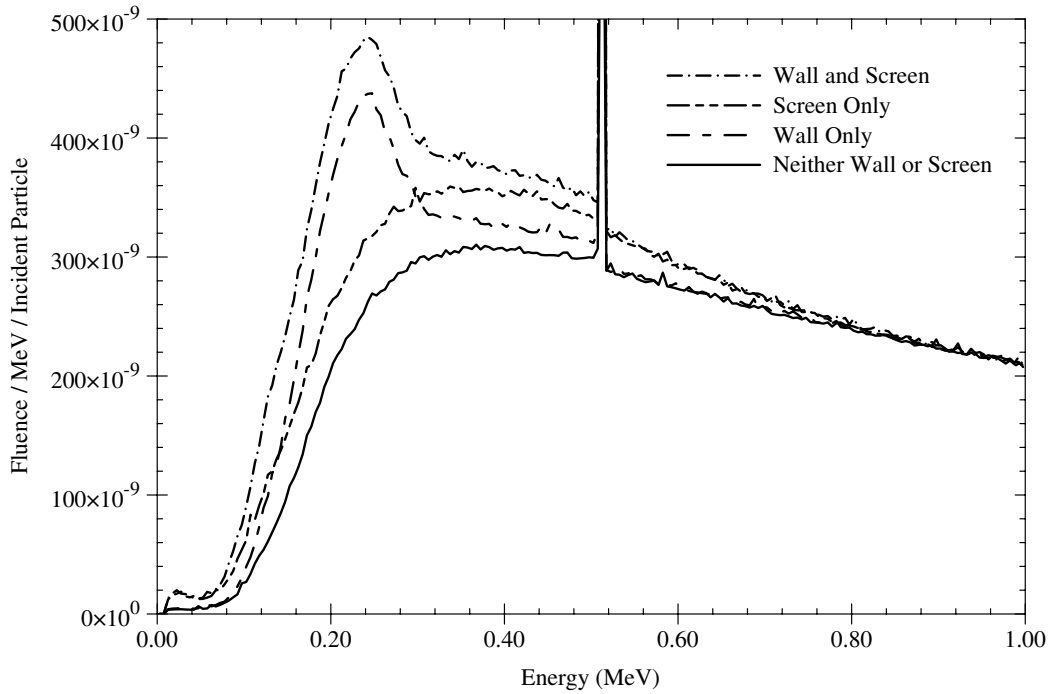

Figure 3.18: All-particle energy spectra (0.0 - 1.0 MeV) at 400 cm SSPD

The Backscatter Peak

Using the phasespace filtering techniques described in Section 2.2.3, energy spectra of backscattered particles were calculated. Figure 3.19, Figure 3.20 and Figure 3.21 show the backscatter energy spectra at 200 cm, 300 cm and 400 cm respectively between 0.0 and 0.5 MeV. The same four screen-wall geometry combinations described in Section 2.2.3 were examined.

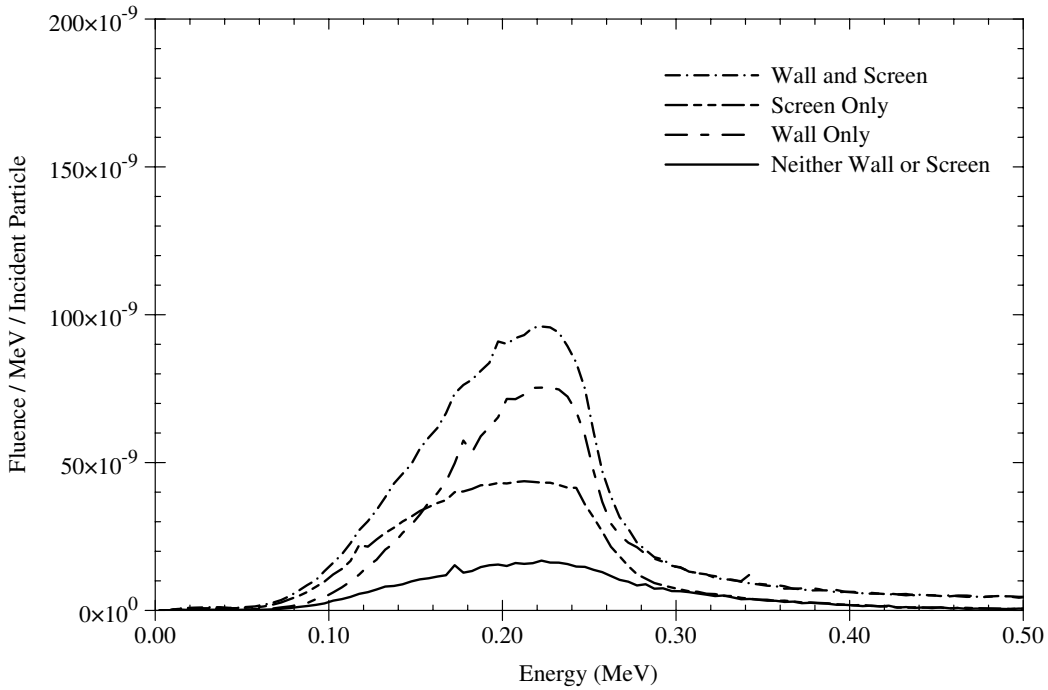

Figure 3.19: All-particle backscatter energy spectra (0.0 - 0.5 MeV) at 200 cm SSPD. For the range of 0.0 - 0.5 MeV, backscattered particles represent % of all particles in the beam.

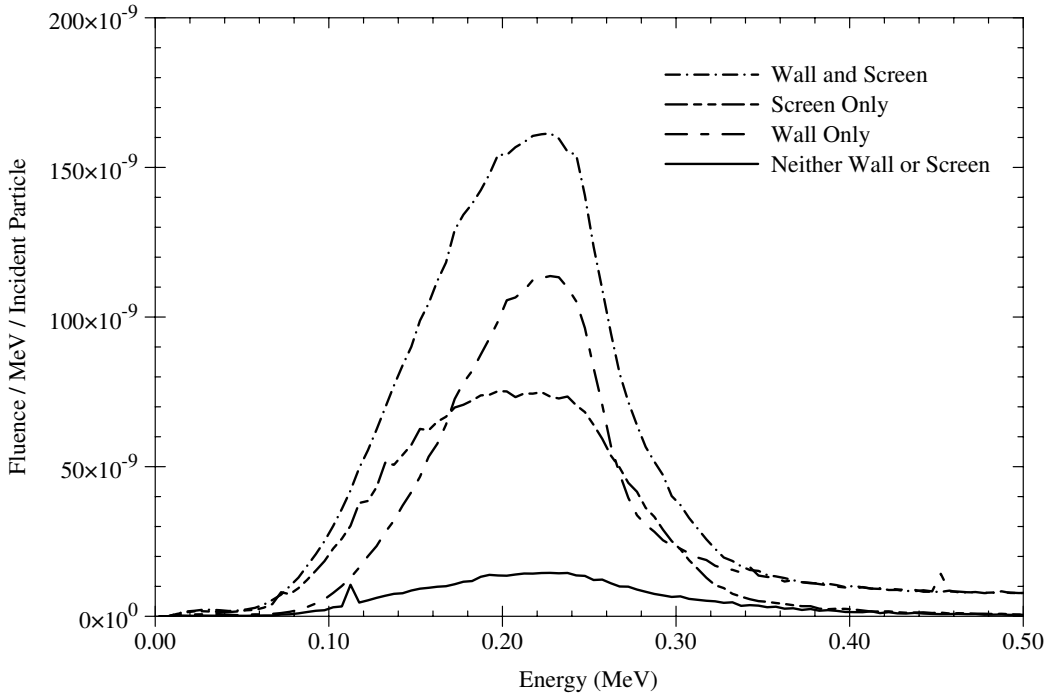

Figure 3.20: All-particle backscatter energy spectra (0.0 - 0.5 MeV) at 300 cm SSPD

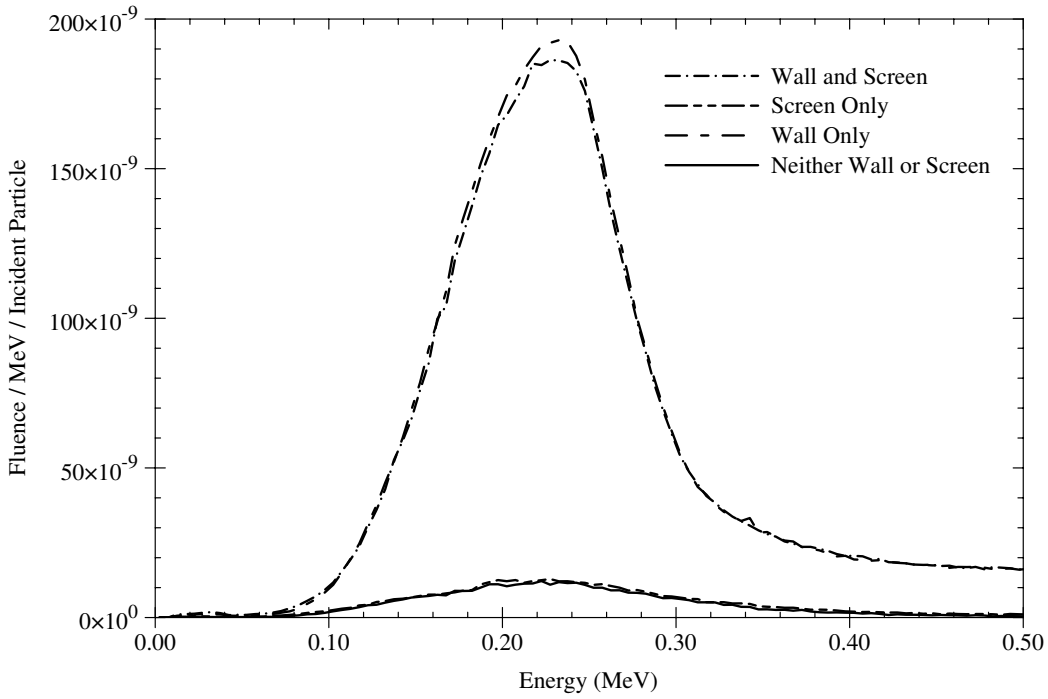

Figure 3.21: All-particle backscatter energy spectra (0.0 - 0.5 MeV) at 400 cm SSPD

In each of the backscatter spectra, backscatter occurred in the models without either the wall or PMMA screen. This backscatter was generated in the column of air behind each scoring plane. For scoring planes in front of the PMMA screen, backscatter from the wall was slightly shielded by the PMMA screen when it was included in the model. A moderate amount of backscatter at these same SSPD's was also created by the PMMA screen itself. At 400 cm SSPD, the only scoring plane positioned downstream of the PMMA screen, scatter from the wall is slightly reduced when the screen is included in the model due to shielding of the primary beam. Table 3.1 shows the fraction of backscattered particles in the beam between the energies of 0.0 and 0.5 MeV for the SSPD's of 200 cm, 300 cm and 400 cm.

Wall or Screen	200 cm	300 cm	400 cm
Wall & Screen	0.059	0.105	0.118
Wall	0.047	0.073	0.133
Screen	0.029	0.054	0.010
Neither	0.012	0.012	0.010

Table 3.1: Fraction of backscattered particles in the beam between the energies of 0.0 and 0.5 MeV for the SSPD's of 200 cm, 300 cm and 400 cm.

Electron Contamination

The purpose of the PMMA screen is to increase to percentage of forward scattered electrons in the beam, to increase the entrance dose to the phantom and improve dose uniformity

with increasing depth. Figure 3.22 shows a 35% increase in the number of forward scattered electrons in the beam at the 400 cm SSPD behind the position of the PMMA screen. The electron energy spectra do not vary with SSD, which agrees with work conduced by Kassaee et al. [4] for 15 MeV photons.

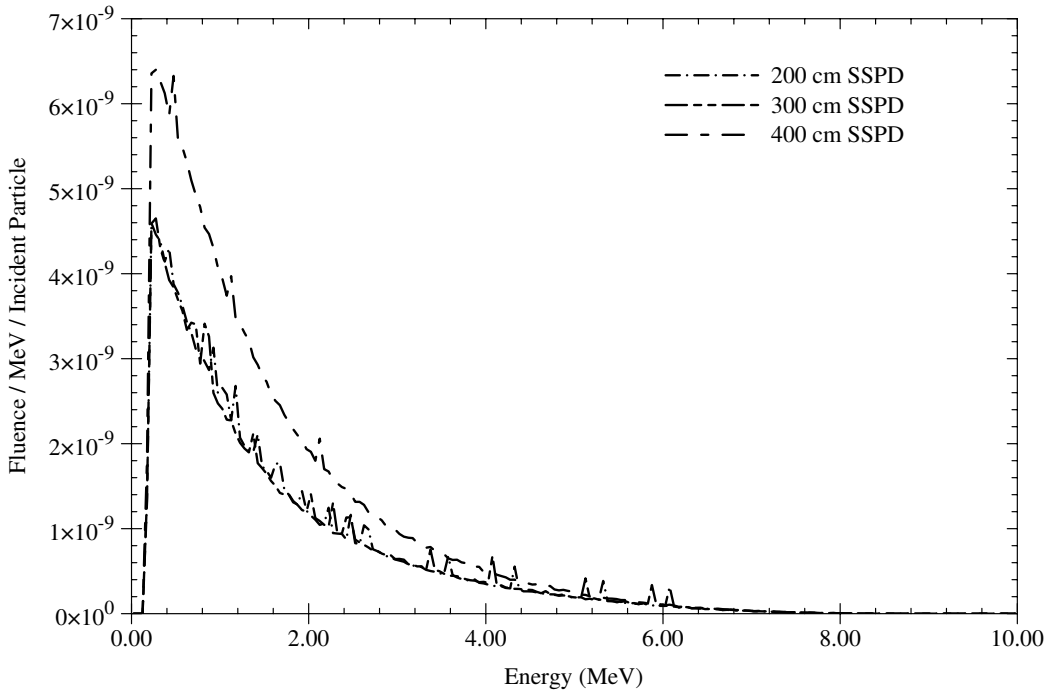

Figure 3.22: Forward scattered electron energy spectra (0.0 - 10.0 MeV) at 200, 300 and 400 cm SSPD with both the PMMA screen and wall included in the model.

Figure 3.23 highlights the influence of including the concrete wall in the model after the 400 cm SSPD scoring plane. Adding the wall appears to increase the number of scattered electrons at the 400 cm SSPD scoring plane.

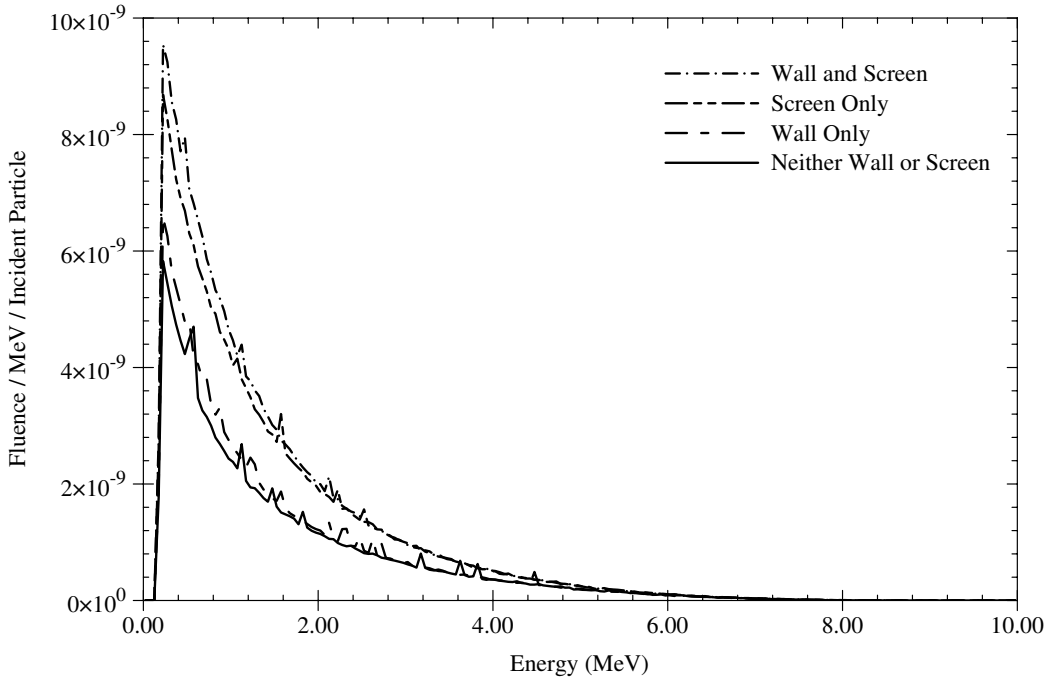

Figure 3.23: Electron energy spectra (0.0 - 10.0 MeV) at 400 cm SSPD including both forward and backscattered electrons.

Chapter 4

Discussion

Simulation of isocentric radiotherapy treatments prior to treatment is routine. Planning for a total body irradiation (TBI) treatment however, is almost invariably performed with manual calculation. This work examines the performance of using Monte Carlo (MC) to predict dose at Extended Source to Surface Distance (ESSD).

A method used to measure depth doses in plastic phantoms was devised. By examining the data in Figure 3.1, it can be seen that the dose to the volume at 290 cm SSD is roughly half that at 190 cm; this is as expected considering the inverse square law. While the uncertainty in the dose measurements is quite low, it is the uncertainty associated with setup that negatively impacts on the usefulness of this method for acquiring depth doses.

Experimentally quantifying the backscatter from the concrete wall to the rear of the treatment area, by shielding the ion-chamber from the primary beam with lead, showed that its contribution to dose in a volume at ESSD was low. At least one quarter of the backscatter signal was cable signal. There is not enough data to properly distinguish between the true backscatter signal and the cable signal.

Exploring the affects of variance reduction is critical in producing an efficient and precise Monte Carlo model. When evaluating the affect a particular technique has on model precision, it is important to be aware of what is being compromised in order to make some efficiency gain or reduction in variance. Range rejection is a good example of a technique that compromises information in an attempt to improve simulation efficiency. To nominate an energy cut-off is to loose all information about a system below that cut-off energy at a particular depth; low energy particles in a simulation that used range rejection would not travel as far though the model compared to a simulation that did not use range rejection. Figure 3.2 clearly shows an increase in model variance with increasing energy cut-off, while there is no significant corresponding reduction in total computation time.

Figure 3.3 shows that photon splitting can greatly reduce the variance in a model without

a significant increase in computation time. A photon splitting number of 5 reduces the variance in a model by a factor of nearly 5.5 while only doubling total simulation time, when compared to a model that does not employ photon splitting. While for very high photon splitting numbers, about 40, the efficiency gain flattens off, there is no model information loss associated with photon splitting; very high photon splitting numbers simply result in a longer computation time. Photon recycling shows a slight trend towards reducing model variance with increasing recycling number (Figure 3.4). This trend is not as pronounced as for photon splitting.

Multi-run averaging is a very subjective variance reduction technique. While it is possible to use this method to reduce the uncertainty of a model, it is very dependant on the order in which a group of models is averaged. The initial random seeds used for the random number generator also affect the performance of this technique. It would be possible to perform a group of simulations, and select only those models with very low variance to average together; for a reduction in model variance of only 20% given a factor of 20 increase in simulation time, multi-run averaging is not efficient.

Including the PMMA build-up screen in the MC model increases the entrance dose to the phantom, this is shown in Figure 3.9. While the entrance dose is increased, the inclusion of the screen tends to reduce the overall dose delivered to the volume at depth. For both models, the high resolution of the build-up region is subject to increased noise; small voxels tend to have fewer particles depositing energy within their volume, this leads to an increase in variance when compared to a large voxel model under the same physical conditions.

Backscatter from the concrete wall at the rear of the treatment area increases the dose delivered to the volume for all depths at an SSD of 400 cm as in Figure 3.10; this difference of 3-5% is within the statistical error of both depth doses. Figure 3.10 does not included the PMMA screen in the model, the difference between the two models all but disappears when the screen is introduced, possibly due to shielding of the primary beam by the PMMA screen; this is shown in Figure 3.11.

The apparent systematic offset between experimental and MC data was reduced from 10% to less than 5% when the experimental data was collected using the polystyrene tower to support the phantom, instead of the steel-framed treatment bed. This highlights the importance of performing experiments that can be modelled accurately. While is it not reasonable to expect all sources of scatter to be included in the model, major objects in the treatment room such as the wall and floor, may be significant sources of scatter at ESSD.

Energy spectra can provide an understanding of the particles that are responsible for delivering dose at a certain location. The full energy spectra shown in Figures 3.13, 3.14 and 3.15 each show a clear peak at 511 keV, corresponding to the rest mass of an electron that

is produced by electron-positron annihilation. With increasing distance from the source, a lower energy peak is seen at 220 keV, this is the backscatter peak. There is evidence in Figure 3.15 that the concrete wall is a major contributor to this backscatter peak.

The low energy spectra of Figures 3.16, 3.17 and 3.18 show the back scatter peak in more detail. The affect of the concrete wall is clear at low energies; it is interesting to note that at 400 cm from the source (down beam of the PMMA screen), the inclusion of the screen in the model further increases the backscatter. The presence of the screen tends reduce the average energy of the beam; beam softening. For energies greater than 1 MeV there is no difference between energy spectra that include or exclude the PMMA screen or the concrete wall; this is true for all SSD's examined. Using the spread of the data in each spectra as an indication of uncertainty in Figures 3.16, 3.16 and 3.18, it can be seen that there is a noticeable reduction in uncertainty with increasing distance from the source; this indicates the proportion of low energy particles in the system increases with increasing distance from the source.

Using readphsp_bs, a modified version of readphsp, readphsp_bs described in Section 2.2.3, the backscatter peak visible in the low energy spectra, was examined in detail by excluding all forward scattered particles from the phasespace files. Figures 3.19 and 3.20 show two energy spectra recorded upstream of the PMMA screen, these two spectra display similar features. It can be seen that the introduction of the concrete wall into the model produces a sharp peak, when compared to the peak created by the PMMA screen alone. In examining the low energy backscatter spectra downstream of the PMMA screen (Figure 3.21), the inclusion of the screen in the model makes no significant difference to the model when the wall is excluded from the model. It does appear however, that the inclusion of the PMMA screen in the model can increase the backscatter from the concrete wall; reinforcing the idea that the screen reduces the average energy of the beam, resulting in more lower energy particles that are more likely to scatter.

Chapter 5

Conclusions & Recommendations

While it is possible to predict the dose to a volume at extended source to surface distance (ESSD) using Monte Carlo (MC), reproducing the scatter conditions present in experimental data is critical. Experimental data at ESSD was collected in a geometry containing many sources of scatter, including the treatment bed and treatment room walls; the cable signal was insignificant in comparison. The MC simulations used were simplified models of the experimental conditions; for comparison to experimental data collected with the treatment bed in the beam, some of these models were not adequate.

Well defined reference conditions proved to be of great value in assessing the MC technique and its performance at ESSD. Ordinarily a depth dose is normalised to d_{max}, if normalisation had been performed in this way for this study, systematic offsets between experiment and MC would have been lost. The use of a reference is also useful in determining if an ESSD model is over or under estimating dose with increasing distance.

Before the MC models were compared to experimental data, their precision was evaluated. Monte Carlo models simulating large geometries tend to require the simulation of very high numbers of particles. In examining a select group of common variance reduction techniques it was shown that photon splitting was most effective in reducing model variance for a comparatively small increase in computation time. photon splitting effectively flooded the models with significantly more photons than would ordinarily be available from a phasespace file of limited size. Using a photon splitting number of between 50 and 70 is adequate for simple rectilinear geometries at ESSD.

Other variance reduction techniques such as range rejection and photon recycling were not as effective. Range rejection increased model variance with increasing energy cut-off, and a high energy cut-off can have a detrimental impact on model integrity. Some information about a system below the cut-off energy is lost for increasing distance away from the source. The use of range rejection should be used only when its impact on a particular model is

well understood; this is especially important if it is low energy particles at depth that are of interest.

Photon recycling and its affect on model variance at ESSD needs further investigation. There is a slight trend towards reducing model variance with increasing recycling number. The effectiveness of this is somewhat limited when compared to that of photon splitting. For a simple geometry, specifying a number of initial histories that is greater than that of the available particles in a phasespace is redundant.

Energy spectra are useful for evaluating the effect beam modifiers have on a system. It can be shown that the PMMA build-up screen does indeed spoil the beam with forward scattered electrons. When the screen is not in place however, the electron contamination of the beam is independent of SSD. Energy spectra are more useful than depth doses in assessing the influence scatter has on a model. The direct examination of backscatter peaks in this study showed nearby objects to the treatment area contribute constructively to the model; rendering it a more accurate reproduction of experimental conditions. This is reinforced by the taking of measurement without the treatment bed in the beam; resulting in an experiment that is simpler to model. Systematic differences between experimental measurements and MC simulations were reduced from 10% to less than 5% by making the experimental measurements on the polystyrene tower rather than the steel framed treatment bed.

In conclusion, using Monte Carlo to model ESSD radiotherapy treatments is feasible, given access to sufficient computing resources. With increasing distance, lower energy particles become more significant in producing robust models. It is important to ensure scatter conditions present under experimental conditions are reproduced accurately. Introducing more particles into a simulation with the use of photon splitting is most effective for reducing model variance. Further investigation needs to be carried out in exploring the performance of MC at ESSD for very high resolution phantoms generated from CT data sets suitable for planning TBI treatments at The Royal Brisbane and Women's Hospital.

Bibliography

[1] S H Levitt, J A Purdy, C A Perez, and S Vijayakumar. *Technical Basis of Radiation Therapy*. Springer-Verlah, Berlin, Heidelberg, 2006.

[2] P Metcalfe, T Kron, and P Hoban. *The Physics of Radiotherapy X-Rays and Electrons*. Medical Physics Publishing, Madison, Wisconsin, 2007.

[3] Susanta K Hui, R K Das, Bruce Thomadsen, and Douglas Henderson. CT-based analysis of dose homogeneity in total body irradiation using lateral beam. *Journal of applied clinical medical physics / American College of Medical Physics*, 5(4):71–9, Mar 2005.

[4] A Kassaee, Y Xiao, P Bloch, J Goldwein, D I Rosenthal, and B E Bjärngard. Doses near the surface during total-body irradiation with 15 MV X-rays. *Int J Cancer*, 96 Suppl:125–30, Jan 2001.

[5] B Sánchez-Nieto, F Sánchez-Doblado, and J Terrón. Computer-based anthropometrical system for total body irradiation. *Medical and Biological Engineering and Computing*, Jan 1997.

[6] Faiz M. Khan. *The Physics of Radiation Therapy*. Lippincott Williams Wilkins, 2003.

[7] T Wheldon. The radiobiological basis of total body irradiation. *British Journal of Radiology*, Jan 1997.

[8] D Gilson and R E Taylor. Total body irradiation. report on a meeting organized by the BIR Oncology Committee, held at The Royal Institute of British Architects, london, 28 november 1996. *The British journal of radiology*, 70(840):1201–3, Dec 1997.

[9] P Sandford. *Verification of Total Body Irradiation Lung Compensators using an EPID*. School of Physical and Chemical Sciences, QUT, 2005.

[10] D Cassidy, A L Fielding, C M Poole, and T Kairn. *RBWH-QUT Research Meeting Minutes*. 14-02-2008.

[11] E Atanassov and I Dimov. What Monte Carlo models can do and cannot do efficiently? *Applied Mathematical Modelling*, 32(8):1477–1500, Aug 2008.

[12] Paul J Keall, Jeffrey V Siebers, Bruce Libby, and Radhe Mohan. Determining the incident electron fluence for Monte Carlo-based photon treatment planning using a standard measured data set. *Medical physics*, 30(4):574–82, Apr 2003.

[13] Antonis Tzedakis, John E Damilakis, Michael Mazonakis, John Stratakis, Haralambos Varveris, and Nicholas Gourtsoyiannis. Influence of initial electron beam parameters

on Monte Carlo calculated absorbed dose distributions for radiotherapy photon beams. *Medical physics*, 31(4):907–13, Apr 2004.

[14] I Kawrakow and B R B Walters. Efficient photon beam dose calculations using DOSXYZnrc with BEAMnrc. *Medical physics*, 33(8):3046–56, Aug 2006.

[15] Khaled Aljarrah, Greg C Sharp, Toni Neicu, and Steve B Jiang. Determination of the initial beam parameters in Monte Carlo linac simulation. *Medical physics*, 33(4):850–8, Apr 2006.

[16] B R B Walters and I Kawrakow. A HOWFARLESS option to increase efficiency of homogeneous phantom calculations with DOSXYZnrc. *Medical physics*, 34(10):3794–807, Oct 2007.

[17] Indrin J Chetty, Bruce Curran, Joanna E Cygler, John J DeMarco, Gary Ezzell, Bruce A Faddegon, Iwan Kawrakow, Paul J Keall, Helen Liu, C M Charlie Ma, D W O Rogers, Jan Seuntjens, Daryoush Sheikh-Bagheri, and Jeffrey V Siebers. Report of the AAPM Task Group no. 105: issues associated with clinical implementation of Monte Carlo-based photon and electron external beam treatment planning. *Med Phys*, 34(12):4818–4853, 2007.

[18] I Kawrakow, D W O Rogers, and B R B Walters. Large efficiency improvements in BEAMnrc using directional bremsstrahlung splitting. *Medical physics*, 31(10):2883–98, Oct 2004.

[19] I Kawrakow. The effect of Monte Carlo statistical uncertainties on the evaluation of dose distributions in radiation treatment planning. *Physics in medicine and biology*, 49(8):1549–56, Apr 2004.

[20] D W Rogers. The role of Monte Carlo simulation of electron transport in radiation dosimetry. *International journal of radiation applications and instrumentation Part A, Applied radiation and isotopes*, 42(10):965–74, Jan 1991.

[21] D W O Rogers, B Walters, and I Kawrakow. *BEAMnrc Users Manual*. National Research Council of Canada, 2006.

[22] B Walters, I Kawrakow, and D W O Rogers. *DOSXYZnrc Users Manual*. National Research Council of Canada, 2006.

[23] Toni Neicu, Khaled M Aljarrah, and Steve B Jiang. A software tool for 2D/3D visualization and analysis of phase-space data generated by Monte Carlo modelling of medical linear accelerators. *Physics in medicine and biology*, 50(20):N257–67, Oct 2005.

[24] James M Galvin. *Total Body Irradiation Dosimetry and Practical Considerations*. Thomas Jefferson University Hospital, 2001.

[25] S Stathakis, C Kappas, and N Papanikolaou. Dose calculations with the BEAM Monte Carlo code at extended SSD's. *Proceedings of the 22nd Annual EMBS International Conference*, July 23-28, 2000.

[26] T Kairn, D Cassidy, P M Sandford, and A L Fielding. Radiotherapy treatment verification using radiological thickness measured with an amorphous silicon electronic portal imaging device: Monte carlo simulation and experiment. *Physics in medicine and biology*, 53(14):3903–19, Jul 2008.

[27] D W O Rogers and R Mohan. Questions for comparison of clinical Monte Carlo codes. *XIIIth International Conference on the Use of Computers in Radiation Therapy*, 2000.

[28] T S Markwell. *Contrast Enhancement of EPID Images via Difference Imaging: A Monte Carlo Simulation Study*. School of Physical and Chemical Sciences, QUT, 2008.

[29] Michael K Fix, Paul J Keall, and Jeffrey V Siebers. Photon-beam subsource sensitivity to the initial electron-beam parameters. *Medical physics*, 32(4):1164–75, Apr 2005.